

# Surface textures of detrital pyroxenes in coastal dune sands (western Gulf of Mexico, Mexico): Implications for their preservation and geoenvironmental processes

Juan J. Kasper-Zubillaga<sup>1</sup>  | Raymundo Gerardo Martínez-Serrano<sup>2</sup> |  
David M. Buchs<sup>3</sup> | Mauricio Mendieta-Lora<sup>4</sup> | Elsa Arellano-Torres<sup>5</sup> |  
León Felipe Álvarez-Sánchez<sup>6</sup>

<sup>1</sup>Instituto de Ciencias del Mar y Limnología (ICMyL), Unidad Académica de Procesos Oceánicos y Costeros, Universidad Nacional Autónoma de México (UNAM), Mexico City, Mexico

<sup>2</sup>Instituto de Geofísica, Laboratorio Universitario de Geoquímica Isotópica, Universidad Nacional Autónoma de México (UNAM), Mexico City, Mexico

<sup>3</sup>School of Earth and Environmental Sciences, Cardiff University, Cardiff, UK

<sup>4</sup>Posgrado en Ciencias del Mar y Limnología, Instituto de Ciencias del Mar y Limnología. Unidad Académica de Procesos Oceánicos y Costeros, Universidad Nacional Autónoma de México (UNAM), Mexico City, Mexico

<sup>5</sup>Facultad de Ciencias, Departamento de Ecología y Recursos Naturales, Universidad Nacional Autónoma de México (UNAM), Mexico City, Mexico

<sup>6</sup>Instituto de Ciencias del Mar y Limnología (ICMyL), Unidad de Informática Marina (UNINMAR), Universidad Nacional Autónoma de México (UNAM), Ciudad Universitaria s/n, Mexico City, Mexico

## Correspondence

Juan J. Kasper-Zubillaga, Instituto de Ciencias del Mar y Limnología (ICMyL), Unidad Académica de Procesos Oceánicos y Costeros, Universidad Nacional Autónoma de México (UNAM), Ciudad Universitaria s/n, 04510 CDMX, Mexico.  
Email: [kasper@cmarl.unam.mx](mailto:kasper@cmarl.unam.mx)

## Funding information

Universidad Nacional Autónoma de México, Grant/Award Number: PASPA/DGAPA/UNAM

## Abstract

This work investigates how the surface textures and morphology of pyroxene grains evolve during their source-to-sink history. This study applies to detrital clinopyroxenes concentrated in coastal dune sands of the Gulf of Mexico which were sourced in the Trans Mexican Volcanic Belt then transported and deposited in environments subject to limited chemical weathering. The composition and morphology of the pyroxenes was characterised using single-grain geochemical analysis and surface texture imagery with a novel approach based on the compactness property to assess the shape of minerals. This reveals heterogeneous diopside-augite populations, displaying mineral morphologies dominantly controlled by impact breakage along cleavages, little physical abrasion along their edges and with limited evidence for chemical weathering. Mechanical surface textures dominate over mechanical/chemical and chemical surface textures. These mechanical surface textures are preserved primarily as flat cleavage surfaces and rounded edges inherited from fluvial-intertidal and aeolian transport, respectively. Mechanically/chemically induced surface textures are preserved as elongated depressions. Chemical surface textures are sparse and mostly represented by mammillated textures that suggest local dissolution under subaqueous

This is an open access article under the terms of the [Creative Commons Attribution](https://creativecommons.org/licenses/by/4.0/) License, which permits use, distribution and reproduction in any medium, provided the original work is properly cited.

© 2023 The Authors. *The Depositional Record* published by John Wiley & Sons Ltd on behalf of International Association of Sedimentologists.

conditions. The scarcity of chemical surface textures is attributed to frequent fragmentation of the clinopyroxenes along cleavages and limited chemical weathering during transport of the observed populations. Clinopyroxene grains in the coastal dune sands primarily retain surface characteristics from fluvial transport. Although the breakage of minerals along cleavages can obscure their original morphology under a weathering-limited erosion regime, this study shows how surface textures and morphology of pyroxene grains is used to determine episodes of transport and deposition close to volcanic environments. The use of the compactness property as a shape descriptor measurement of particles provides an alternative approach to observe how clinopyroxene remains unaltered despite the high energy conditions of the coastal area.

#### KEYWORDS

clinopyroxene, coastal dune sands, compactness, Mexico, surface textures, weathering

## 1 | INTRODUCTION

Surface textures on quartz and heavy minerals have been commonly used to assess the transport and depositional mechanisms grains experienced throughout their sedimentary cycles in ancient and recent fluvial, marine and aeolian environments (Armstrong-Altrin & Pineda-Olmedo, 2014; Costa et al., 2013; Dott, 2003; Gravenor & Leavitt, 1981; Itamiya et al., 2019; Kasper-Zubillaga et al., 2005; Krinsley et al., 1976; Krinsley & Donahue, 1968; Madhavaraju et al., 2022; Mejía-Ledezma et al., 2020; Phillips-Lander et al., 2017). In contrast to quartz (Costa et al., 2019; Immonen, 2013; Krinsley & Doornkamp, 1973; Mahaney, 2002; Vos et al., 2014) and heavy minerals (Mejía-Ledezma et al., 2020; Moral-Cardona et al., 2005; Velbel et al., 2007; Velbel & Ranck, 2008), surface textures on pyroxene grains are reported to be useful as indicators of weathering and mechanical abrasion (Andò et al., 2012; Garzanti et al., 2015a, 2015b; Le Pera & Morrone, 2020; Morrone et al., 2020; Schott et al., 1981; Velbel, 2007) in ancient and recent sands. Similar to other ferromagnesian minerals, pyroxene grains can be rare in sands due to their vulnerability to chemical weathering and diagenesis (Deer et al., 1992; Delvigne, 1990; Marsaglia, 1993; Schott et al., 1981; Velbel & Barker, 2008), but they are nonetheless commonly found in volcanoclastic sediments (Hamill & Ballance, 1985; Le Pera et al., 2021). Even after long distance energetic subaquatic and subaerial conditions pyroxene can survive as part of the compositional framework of coastal sands (Garzanti et al., 2014, 2015a, 2018, 2021, 2022).

Hence, surface textures on clinopyroxenes offer the opportunity to identify some of the physical and chemical mechanisms that enable pyroxene grains to survive in a sandy coastal area emplaced within a volcanoclastic environment.

Along with the microtextural record, it is well known that the morphology of detrital minerals (e.g. sphericity/roundness/angulosity) are inherited grain properties determined by mechanical and chemical processes during the sedimentary cycle (Costa et al., 2013; Folk, 1980; Grandstaff, 1978; Immonen, 2013; Krinsley & Wellendorf, 1980; Resentini et al., 2018; Zhao & Wang, 2016). In addition, the morphology of pyroxenes can be primarily controlled by their weak cleavage surface boundaries and vulnerability to chemical weathering under natural and artificial conditions (Andò et al., 2012; Garzanti et al., 2015a, 2015b; Le Pera & Morrone, 2020; Velbel, 2007). However, there are only a few studies providing detailed constraints on these processes and their record in the morphology of pyroxenes. This paper addresses this issue by investigating the composition and morphology of detrital pyroxenes collected in fine-grained, well-sorted, litho-quartzose modern sand dunes deposited under moderate chemical weathering within the Gulf of Mexico coastal plain in Mexico, which record volcanoclastic supply from the nearby Trans Mexican Volcanic Belt (Mejía-Ledezma et al., 2020; Mendieta-Lora et al., 2018). Quantitative analyses to determine the composition of the pyroxene were carried out by energy dispersive spectrometers (EDS) and wavelength-dispersive spectrometers (WDS) with a peak counting time of 10s for Na and K. To determine the morphology of the pyroxenes the compactness shape descriptor property of objects was used to assess the shape of a sand-sized mineral closely related to a circle in the Euclidean domain or a polygon in the digital domain (Bogaert et al., 2000; Bribiesca, 2000; Li et al., 2013; Montero & Bribiesca, 2009; Osserman, 1978; Roduit, 2019). Hence, compactness offers an alternative

way to describe the shape of the grains utilising the properties of sphericity and convexity (see Bufham, 2000; Zhao & Wang, 2016). This approach can be regarded as an alternative to Fourier coefficient image analysis (Diepenbroek et al., 1992; Resentini et al., 2018; Thomas et al., 1995) and fractal analysis of grains (Hyslip & Vallejo, 1997; Maria & Carey, 2002, 2007; Zhou et al., 2018) to quantify the shape of sediment particles.

## 2 | STUDY AREA

The study area is located in the state of Veracruz along the western Gulf of Mexico, Mexico. It is part of the coastal area and the Maya Terrane (20°12', 19°24'N; 96°45', 96°19'W; Centeno-García, 2016; Tamayo, 2013; Figures 1 and 2). The climate is defined as Am (warm-humid with a summer rainfall maxima) and Aw (sub-humid with summer rainfall; Kottek et al., 2006). Intense tropical storms are common from June to November (Tamayo, 2013), with low air temperatures between 17 and 25°C and highs of 22–30°C. The average precipitation ranges from 370 mm in summer to 60 mm in winter. The annual average humidity is about 80% (Tejeda et al., 1988).

### 2.1 | Coastal features and fluvial network

The Gulf of Mexico coastal plain is a wave-dominated, transgressive, low relief, narrow coastal plain, averaging 1.25 km in width (Ortiz-Pérez & Espinosa, 1991). Hinterland rivers are derived from the inactive volcanic complex of the Trans Mexican Volcanic Belt. Rivers developed as dendritic and subparallel arrangements of permanent and intermittent discharges (Figure 2).

Perennial rivers include the larger Cazonas and Actopan rivers with drainage basins of 2688 and 2100 km<sup>2</sup>, respectively (Mejía-Ledezma et al., 2020; Pereyra Díaz et al., 2010; Pérez-Quezadas et al., 2017). Conversely, the Boca de Ovejas, Palma Sola and El Viejón rivers flow intermittently with insignificant drainage basins located in the central area of the western Gulf of Mexico coastal plain (Kasper-Zubillaga et al., 1999).

### 2.2 | Physical oceanography and wind regime

The longshore drift is characterised by a northward component in spring–summer with velocities of 0.035–0.08 m/s (Fernández-Eguiarte et al., 1992). The average wave height is 0.90 m with 3–8 s periods. The tidal regime

in the western Gulf of Mexico is negligible. Tides of diurnal and mixed-diurnal types have an average tidal range of 0.30 m. Winds come from the north, east, north-east and south-east with maximum velocities of 4–5 m/s (Mejía-Ledezma et al., 2020; Pérez-Villegas, 1990).

### 2.3 | Geological setting

The Trans Mexican Volcanic Belt Neogene continental arc is a volcanic province *ca* 1000 km long with a width of *ca* 80 to 230 km (Ferrari et al., 2011; Servicio Geológico Mexicano, 2017). It follows an E–W direction in its central and eastern parts. In its western sector, the belt develops a WNW–ESE trend with an angle of *ca* 16° with the Middle America Trench (Demant, 1979; Gómez-Tuena et al., 2007). The Trans Mexican Volcanic Belt divides the central part of Mexico into three sectors, from the Mexican Pacific to the Gulf of Mexico coasts (Alaniz-Alvarez et al., 2002; Demant, 1979; Pasquaré et al., 1991).

In the Gulf of Mexico coastal plain, the rocks of the Trans Mexican Volcanic Belt are compositionally dominated by mafic, intermediate and acid rocks exposed as basalts, andesites, andesite-dacites and basalt-rhyolite tuffs of Miocene and Pliocene ages (Ferrari et al., 2011; Servicio Geológico Mexicano, 2017). Miocene andesites are the oldest Trans Mexican Volcanic Belt rocks exposed along the coast. Basalts and basaltic breccias represent upper Miocene to lower Pliocene rocks of mugearitic composition (e.g. Na-alkaline structure exposed at the Palma Sola coastal area; Figure 1). These rocks contain phenocrysts of plagioclase, augite-diopside, oligoclase, opaque minerals and olivine suites (Ferrari et al., 2005; Gómez-Tuena et al., 2007). The upper Pliocene to Quaternary volcanic rocks are of calc-alkaline composition (Ferrari et al., 2005; Gómez-Tuena et al., 2007; Negendank et al., 1985; Figure 1). Recent units are exposed as Plio-Quaternary alluvial deposits and dune fields occur along the coastal area (Ferrari et al., 2005).

### 2.4 | Dune fields

Dune fields cover an extensive coastal area throughout the Gulf of Mexico coastal plain including transverse mobile and vegetated dunes with average heights of 2–8 m in the north-central coastal area, that is Istiríncha (I) to Boca Andrea (BA). In contrast, the coastal dunes in the south, that is Villa Rica (VR) to Chachalacas (CH), are transverse-vegetated, parabolic and barchan coastal dunes with average heights of *ca* 10 m (Mendieta-Lora et al., 2018; Figures 1 and 3A,B,C). The dunes are exposed where chemical weathering action is lower than sand transport rates (Johnsson et al., 1993; Kasper-Zubillaga et al., 2022).



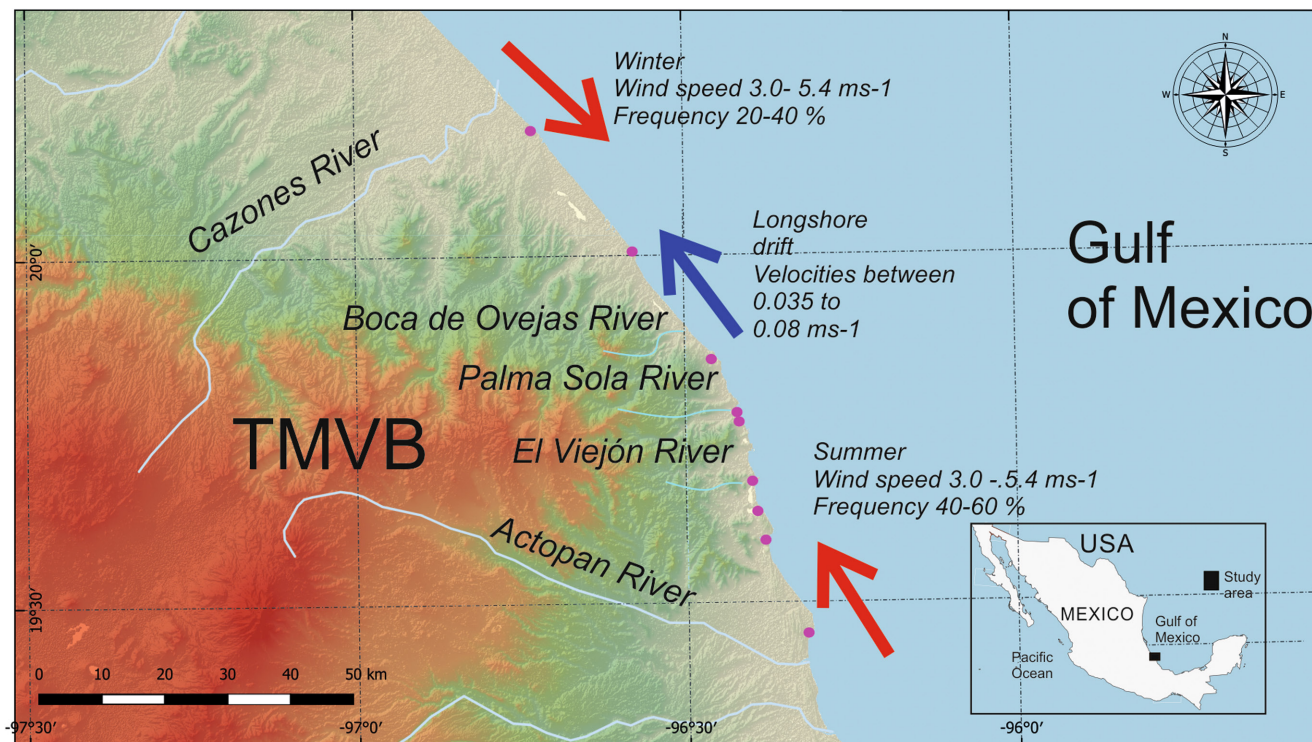


**FIGURE 2** Dominant north-westerly, south-easterly winds, long shore drift and fluvial network along the Gulf of Mexico coastal plain. Cazones and Actopan are perennial rivers whereas Boca de Ovejas, Palma Sola and El Viejón are intermittent rivers (modified from Kasper-Zubillaga et al., 2022).

sediments were collected away from anomalous heavy-mineral lag-concentration deposits (Garzanti et al., 2015b).

## 3.2 | Scanning electron microscopy analysis

### 3.2.1 | Sample preparation and geochemical analyses

Samples were cleaned and rinsed with distilled water, avoiding chemical solutions that might remove adhering particles since they provide valuable information on the surface texture attributes of the grains (Vos et al., 2014). After cleaning, the sands were dried in an oven at 50°C. A small amount of the whole bulk sand sample (*ca* 0.5 g) was placed in a Petri-like dish under a binocular microscope objective 4X-Velab-VES1 for separation of pyroxene grains by hand-picking based on their noticeable green and dark green colour and shape. Pyroxene grains ranging from 100 µm to 2 mm, suitable for assessing the prevailing surface textures (Vos et al., 2014), were separated from bulk samples of very fine to fine sand (from 2.5 to 3.0 φ). This grain size consideration was achieved after most of the grains observed were bigger than 100 µm (e.g. 2.5–3.0 φ; very fine to fine sands).

A selection of separated crystals were mounted on organic resin slides, polished, and coated with graphite.

The centre of each pyroxene crystal was then analysed twice by electron microprobe ( $n = 66$ ) (Figure 4A through E). The geochemical characterisation of pyroxene minerals in sand samples can be carried out by EDS or WDS. The EDS technique is relatively fast and enables almost simultaneous determination of the chemical elements that compose a mineral sample, although with lower precision. However, the WDS analysis is more suitable for ferromagnesian phases because more detailed information is obtained in terms of chemical composition that can be related to the source rock of the pyroxene grains. The WDS analysis is not as fast as EDS but has better precision since only one element can be monitored at a time in each spectrometer, although the parallel acquisition of  $n$  elements ( $n \dots$  number of spectrometers) is achieved.

An automated JEOL JXA8900-R electron microprobe with five WDS and one EDS was employed (Laboratorio Universitario de Petrología, Universidad Nacional Autónoma de México, UNAM). An acceleration voltage of 20 keV and 20 nA current with a 1.0 µm beam diameter was used. Quantitative analyses were carried out by WDS with a peak counting time of 10 s for Na and K, and 30 s for the other elements. Calibration was performed using international standards (United States Geological Survey; USGS) and internal standards (Division of Structure Probe, Inc.; SPI). Matrix effects were corrected for using the JEOL-ZAF protocol, with the maximum analytical error in oxides

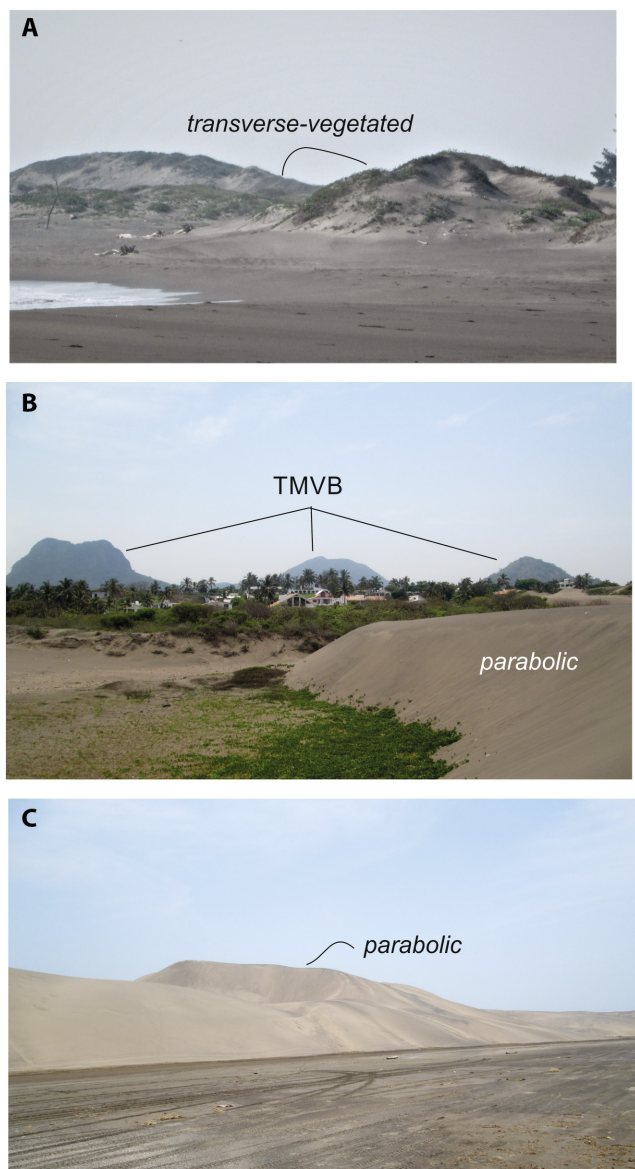


**FIGURE 3** Some coastal dune systems are: (A) El Morro transverse vegetated, (B) Villa Rica parabolic and (C) Chachalacas parabolic dune systems.

determined to be less than 3%. The quality of the data was assessed using kaersulite, olivine, diopside, cuprite and pentlandite standards. Only analyses with a total >96 wt% were considered valid (most of the analytical totals range between 98 and 101 wt%, as expected for pyroxenes). The structural formula of the pyroxenes was calculated according to the method described in Morimoto et al. (1988).

### 3.2.2 | Grain shape assessment: Compactness measurements

Quantitative measurement of compactness on pyroxene grains was obtained from petrographic images

using the J Microvision v. 1.3.4 software ( $n = 332$  grains; Roduit, 2019). The compactness property of objects and particles has been widely used to quantify the extent to which a geographical area changes throughout space and time (Bogaert et al., 2000; Bribiesca, 2000; Chaudhuri et al., 2012; Li et al., 2013). To date, compactness measurements have been used to assess the shapes of objects without any attempt to employ them as shape descriptors in minerals. This study aims to discuss how pyroxene grains are mechanically and chemically altered during transport and deposition using the compactness shape property. Compactness for isoperimetric inequality ratios is defined as the ratio of the area of the object to the size of a circle with the same perimeter.

$$C = 4\pi A / P^2$$

where  $C$  represents the compactness,  $A$  represents the area of the particle and  $P^2$  represents the squared perimeter of any object (Li et al., 2013; Osserman, 1978). Compactness in grains is an alternative method implemented to quantify particle shape. Quantification involves determining the area of the enclosing sphere ( $4\pi A$ ) that contains the particle's perimeter ( $P$ ). Compactness measurements encompass (i) sphericity, defined as the ratio of the surface area of a sphere with the same volume as the given particle to the surface area of the particle (Wadell, 1932) and the (ii) convexity, defined as the ratio of the volume of a particle and the volume of the convex hull that is the smallest polygon that contains a set of points inside it where interior angles of the convex polygon are  $\leq 180^\circ$  (see Angelidakis et al., 2022; Graham & Yao, 1983; Montero & Bribiesca, 2009; Zhao & Wang, 2016). Hence, compactness compares the particle with its volume equivalent sphere whereas convexity is a measure of the smallest set of convex shapes of the particle approaching a polygon (Zhao & Wang, 2016). Roundness is excluded as a parameter to define compactness measurements since roundness measurements determine the corners and sharpness of the grains whereas compactness accounts for the overall shape close to a circle. Furthermore, shape compactness, sphericity and circularity are the same concepts in a continuous plane and 3D shape in Euclidean spaces (Montero & Bribiesca, 2009). Nonetheless, compactness values in the digital domain can be interpreted in terms of the shape of the clinopyroxene once the crystal suffers breakage and its morphology tends to a polygon rather than a circle (see Rosenfeld, 1974). To assess the compactness of pyroxene grains, the JMicrovision software allows binary images to be analysed accurately by pixel connectivity, extraction and digitalisation of the grains following the pixel codes arrangement based on Freeman (1961) and the empirical formula for perimeter (Vossepoel & Smeulders, 1982). In binary images, white regions represent the foreground pixels

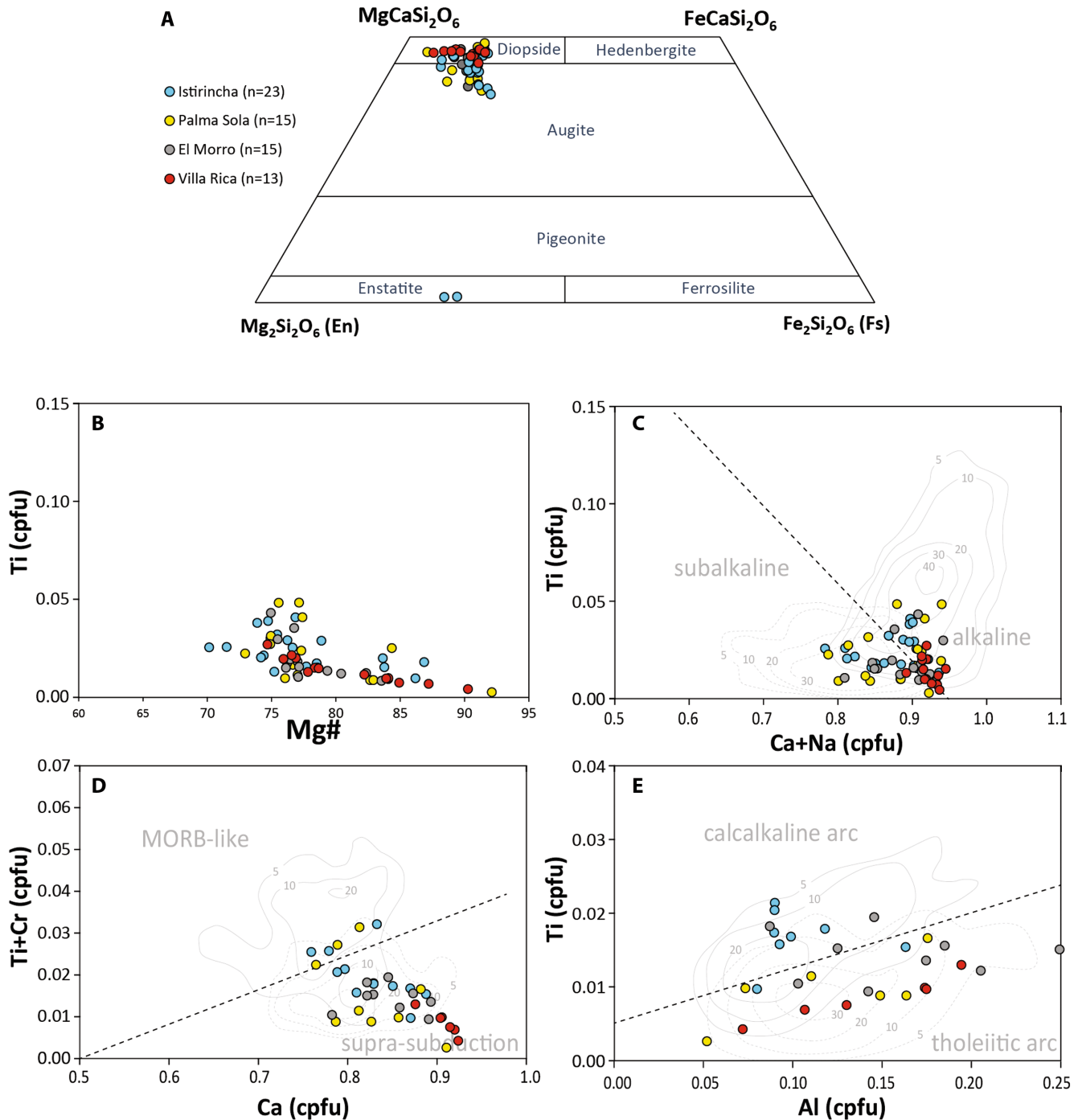


**FIGURE 4** (A) Geochemical composition of pyroxene grains by electron microprobe ( $n=66$ ) (Morimoto et al., 1988). Magmatic differentiation of source rocks based on the geochemical composition of calcic clinopyroxenes (see Letierrier et al., 1982), (B) Mg versus Ti (cpfu), (C) Ca + Na (cpfu) versus Ti (cpfu), (D) Ca (cpfu) versus Ti + Cr (cpfu), (E) Al (cpfu) versus Ti (cpfu).

in 8-pixel connectivity and black regions the background pixels in 4-pixel connectivity.

A database of compactness resulted from: (a) the spatial calibration of the grains in microns; (b) the extraction operation to configure the grain images (image segmentation); (c) adjustment of the surface filters to ensure a 1000 pixel value to compute the descriptors of the grain's shape; (d) removal of the border and fill filters to avoid adjacent

objects from the grain's border contour and surface holes and (e) the image threshold operation to convert the original greyscale image into a binary image (see Roudit, 2019). Compactness measurements range from 0.00 to 1.00, defined as low to high compactness (Li et al., 2013; Montero & Bribiesca, 2009; Roudit, 2019). Limitations with the compactness measurements of particles in the digital domain still remains a problem as they present fractal

patterns which might lead to dissimilar compactness values (Bribiesca, 2000; Rosenfeld, 1974). To ensure as much as possible the consistency of this compactness data, a visual inspection calibration of the grains was performed providing a full catalogue of dissimilar shapes of clinopyroxene (see Supplementary data available at <https://hdl.handle.net/20.500.12201/11352>).

Additional shape parameters like sphericity, convexity and roundness were obtained to observe any significant changes in the grain shape patterns of the clinopyroxenes and evaluate the value of the compactness parameter relative to more traditional approaches. Sphericity values were obtained following the sphericity index  $I_s = A_1/A$ , where  $A_1$  is the area of the maximum inscribed circle obtained from the width of the particle (minimum radius) and  $A$  the particle area of the covering circle computed by the length of the particle (maximum radius; see Mo, 2020) (Table 1). Convexity values were obtained from the JMicrovision software descriptor shape output data based on the convexity hull (Zhao & Wang, 2016; Table 1). Roundness values were obtained by visual inspection of the SEM images based on the chart by Resentini et al. (2018, from figure 4; Table 1; Supplementary data available at <https://hdl.handle.net/20.500.12201/11352>).

### 3.2.3 | Scanning electron microscopy imaging of pyroxenes

A total of 337 pyroxene grains from 32 samples were observed using a SEM-Jeol-JSM 6360LV at the Instituto de Ciencias del Mar y Limnología, UNAM, Mexico.

Grains were mounted on a specimen holder to be observed on an X-Y-Z tilt rotation stage and coated with gold for the best resolution (i.e. when compared to other metals or carbon; Krinsley & Doorkamp, 1973). A working distance of 15 mm was used for 200× magnification. A voltage of 10 kV was obtained using a tungsten filament in high vacuum mode.

### 3.2.4 | Quantitative assessment of surface textures

The percentage of total grain's pixel coverage area for each surface texture on the pyroxene crystal was assessed by the JMicrovision v. 1.3.4 software. This was done by using one single polygon interaction around the image's external boundary to reduce the number of edges and preserve the grain's contour as much as possible (see Chaudhuri et al., 2012; Ramer, 1972; Roduit, 2007). Each polygon represents the surface area on the grain's total area equivalent to 100% of the pyroxene crystal.

The measurements were first obtained from a scale calibration set up in millimetres on the image. The contouring of each individual grain was achieved manually by drawing an iterative selection of a subset of points as vertices of a polygon on the silhouette image for each pyroxene image using the 2D setup tool from the J Microvision v. 1.3.4 software (Roduit, 2019). The same contouring procedure was applied for each surface texture covering the grain's surface. Finally, for each surface texture, a percent proportion expressed as a percent value of the area covered is obtained for each pyroxene grain (Figure 5A through J).

## 4 | RESULTS

### 4.1 | Geochemical composition of pyroxenes

Among the 66 analysed pyroxenes, 64 are clinopyroxenes ranging in composition between diopside and augite, and two are enstatites (Figure 4A). The Mg# (Mg/Mg+Fe×100) of the clinopyroxenes ranges between 70 and 92 (Figure 4B), consistent with the provenance of the minerals from basaltic to andesitic volcanic sources. Titanium increases gradually from approximately 0.003–0.05 cpfu (cation per formula unit), or from 0.1 to 1.7 wt%, with decreasing Mg# (Figure 4B). This trend is consistent with crystallisation in mafic to intermediate melts without the abrupt appearance of Fe-Ti oxides during magmatic differentiation. Variability of Ti at a given Mg# suggests distinct sources for the clinopyroxenes. Accordingly, discrimination of magmatic series using the approach by Leterrier et al. (1982) indicates that the clinopyroxenes predominantly sourced in a volcanic arc, with a subset of grains originating from an alkaline source (Figure 4C,D,E). This is consistent with provenance of the studied volcanoclastic sand from the Trans Mexican Volcanic Belt. No obvious compositional difference was observed between the pyroxenes from distinct sampling localities.

### 4.2 | Compactness, sphericity, convexity and roundness measurements

The average compactness for all coastal sites for the clinopyroxene grains is  $0.71 \pm 0.10$ , the average sphericity value for most of the clinopyroxene grains is  $0.46 \pm 0.20$ , and the average convexity value for most of the grains is  $0.93 \pm 0.06$ . Significant correlations for La Mancha, Villa Rica, Chachalacas, El Moro Farallon and Lechuguillas between compactness and sphericity for clinopyroxene grains are observed (Figure 6A, see Table 1 for the number of samples). A lack of significant correlations

TABLE 1 Average and SD of compactness, sphericity, convexity and roundness in pyroxene grains ( $n = 332$ ).

<b>Istiricha, <math>n = 48</math> grains</b>	<b>I-s1</b>	<b>I-c1</b>	<b>I-c2</b>	<b>I-l</b>
Compactness	$0.68 \pm 0.11$	$0.66 \pm 0.19$	$0.70 \pm 0.08$	$0.72 \pm 0.10$
Sphericity	$0.51 \pm 0.17$	$0.47 \pm 0.25$	$0.40 \pm 0.20$	$0.54 \pm 0.32$
Convexity	$0.90 \pm 0.07$	$0.89 \pm 0.09$	$0.93 \pm 0.04$	$0.94 \pm 0.03$
Roundness	$0.56 \pm 0.13$	$0.60 \pm 0.18$	$0.52 \pm 0.10$	$0.50 \pm 0.09$
<b>Lechuguillas, <math>n = 40</math></b>	<b>Le-s1</b>	<b>Le-c</b>	<b>Le-c1</b>	<b>Le-l2</b>
Compactness	$0.65 \pm 0.10$	$0.65 \pm 0.17$	$0.77 \pm 0.06$	$0.73 \pm 0.09$
Sphericity	$0.32 \pm 0.16$	$0.46 \pm 0.20$	$0.60 \pm 0.19$	$0.52 \pm 0.19$
Convexity	$0.92 \pm 0.05$	$0.88 \pm 0.10$	$0.94 \pm 0.02$	$0.93 \pm 0.05$
Roundness	$0.55 \pm 0.06$	$0.054 \pm 0.06$	$0.50 \pm 0.11$	$0.51 \pm 0.08$
<b>El Morro, <math>n = 44</math></b>	<b>EM-s1</b>	<b>EM-c1</b>	<b>EM-c2</b>	<b>EM-l2</b>
Compactness	$0.70 \pm 0.08$	$0.69 \pm 0.07$	$0.74 \pm 0.07$	$0.73 \pm 0.12$
Sphericity	$0.39 \pm 0.18$	$0.40 \pm 0.18$	$0.40 \pm 0.15$	$0.37 \pm 0.21$
Convexity	$0.94 \pm 0.01$	$0.95 \pm 0.04$	$0.95 \pm 0.02$	$0.97 \pm 0.01$
Roundness	$0.53 \pm 0.10$	$0.54 \pm 0.09$	$0.49 \pm 0.09$	$0.57 \pm 0.10$
<b>Palma Sola, <math>n = 20</math></b>	<b>PS-s1</b>		<b>PS-c1</b>	
Compactness	$0.64 \pm 0.11$		$0.67 \pm 0.09$	
Sphericity	$0.64 \pm 0.18$		$0.58 \pm 0.21$	
Convexity	$0.86 \pm 0.07$		$0.89 \pm 0.06$	
Roundness	$0.48 \pm 0.07$		$0.45 \pm 0.09$	
<b>Boca Andrea, <math>n = 20</math></b>	<b>BA-s</b>		<b>BA-c</b>	
Compactness	$0.61 \pm 0.14$		$0.66 \pm 0.13$	
Sphericity	$0.56 \pm 0.16$		$0.58 \pm 0.11$	
Convexity	$0.85 \pm 0.10$		$0.88 \pm 0.10$	
Roundness	$0.47 \pm 0.08$		$0.49 \pm 0.08$	
<b>Villa Rica, <math>n = 40</math></b>	<b>VR-s1</b>	<b>VR-s2</b>	<b>VR-c</b>	<b>VR-c2</b>
Compactness	$0.77 \pm 0.08$	$0.76 \pm 0.05$	$0.82 \pm 0.07$	$0.73 \pm 0.09$
Sphericity	$0.48 \pm 0.19$	$0.49 \pm 0.17$	$0.67 \pm 0.15$	$0.47 \pm 0.21$
Convexity	$0.96 \pm 0.02$	$0.96 \pm 0.01$	$0.94 \pm 0.03$	$0.94 \pm 0.03$
Roundness	$0.54 \pm 0.08$	$0.58 \pm 0.11$	$0.53 \pm 0.10$	$0.51 \pm 0.06$
<b>El Farallon, <math>n = 40</math></b>	<b>F-s1</b>	<b>F-s</b>	<b>F-c1</b>	<b>F-c</b>
Compactness	$0.75 \pm 0.10$	$0.70 \pm 0.09$	$0.73 \pm 0.08$	$0.67 \pm 0.12$
Sphericity	$0.50 \pm 0.19$	$0.34 \pm 0.19$	$0.35 \pm 0.17$	$0.32 \pm 0.14$
Convexity	$0.94 \pm 0.03$	$0.96 \pm 0.02$	$0.96 \pm 0.03$	$0.92 \pm 0.09$
Roundness	$0.50 \pm 0.06$	$0.62 \pm 0.12$	$0.62 \pm 0.10$	$0.60 \pm 0.08$
<b>La Mancha, <math>n = 40</math></b>	<b>LM-s1</b>	<b>LM-s3</b>	<b>LM-c1</b>	<b>LM-c3</b>
Compactness	$0.68 \pm 0.10$	$0.75 \pm 0.07$	$0.74 \pm 0.11$	$0.78 \pm 0.10$
Sphericity	$0.32 \pm 0.11$	$0.37 \pm 0.17$	$0.49 \pm 0.11$	$0.51 \pm 0.19$
Convexity	$0.93 \pm 0.06$	$0.96 \pm 0.02$	$0.95 \pm 0.07$	$0.96 \pm 0.02$
Roundness	$0.60 \pm 0.07$	$0.53 \pm 0.07$	$0.55 \pm 0.12$	$0.55 \pm 0.10$
<b>Chahalacas, <math>n = 40</math></b>	<b>CH-s</b>	<b>CH-s5</b>	<b>CH-c</b>	<b>CH-c4</b>
Compactness	$0.74 \pm 0.08$	$0.76 \pm 0.08$	$0.71 \pm 0.12$	$0.77 \pm 0.09$

(Continues)

TABLE 1 (Continued)

Chachalacas, <i>n</i> = 40	CH-s	CH-s5	CH-c	CH-c4
Sphericity	0.44 ± 0.19	0.40 ± 0.18	0.36 ± 0.19	0.54 ± 0.21
Convexity	0.94 ± 0.03	0.97 ± 0.01	0.94 ± 0.06	0.94 ± 0.03
Roundness	0.56 ± 0.08	0.58 ± 0.08	0.59 ± 0.06	0.56 ± 0.08

is determined for Boca Andrea, Istirinchá and Palma Sola (Figure S1). Nonetheless, a significant correlation is achieved for most of the samples (Figure 6A). Strong correlations between compactness and convexity are observed for each separate site and for all the sites together (Figure 6B; Figure S2). Finally, a lack of significant correlations exists between compactness and roundness for the clinopyroxene grains at each site and most of the studied areas (Figure 6C; Figure S3). To compare the values of compactness, sphericity and convexity, three images with dissimilar shapes are presented in Figure 7A through C.

### 4.3 | Surface textures in pyroxene grains

For each site, values for the average surface area coverage (%) are represented by mechanical and mechanical-chemical features limited to flat cleavage surfaces with low features Chachalacas (17 ± 16), high features Boca Andrea (77 ± 23); bulbous edges, low features Palma Sola and Boca Andrea (7 ± 13); high features Chachalacas (50 ± 22) and elongated depressions, low features Palma Sola and Boca Andrea (2 ± 6); high features Chachalacas (22 ± 19).

The contribution resulting from grouping mechanical, mechanical-chemical and chemical surface textures for most of the locations, that is Istirinchá + Lechuguillas + El Morro + Palma Sola + Boca Andrea + Villa Rica + Farrallón + La Mancha + Chachalacas, is limited to coverage by the high percentage of flat cleavage surfaces (48 ± 30%), bulbous edges (24 ± 26%) and elongated depressions (10 ± 15%) compared to the rest of the surface textures area coverage.

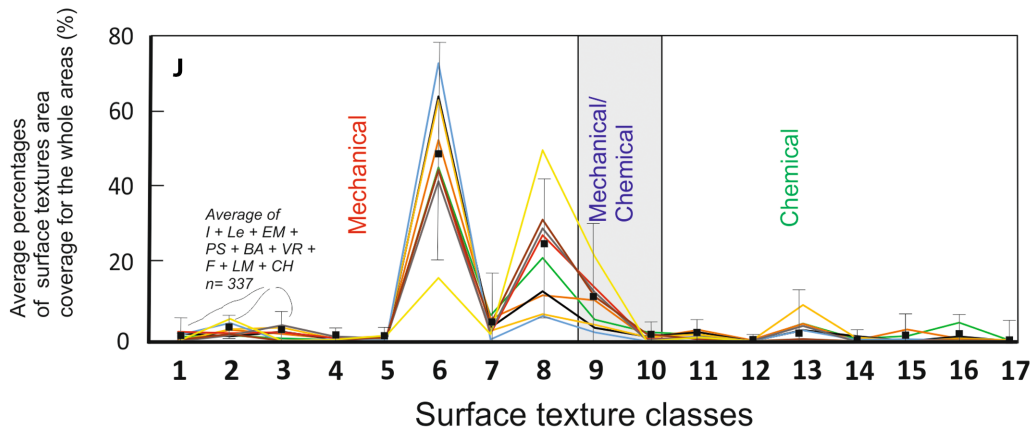
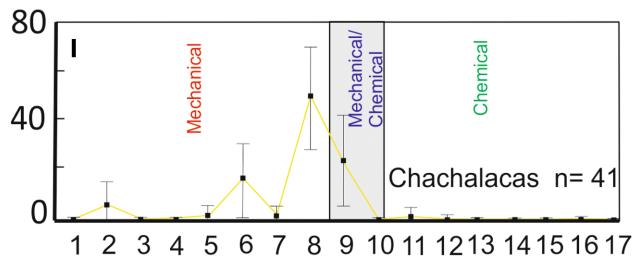
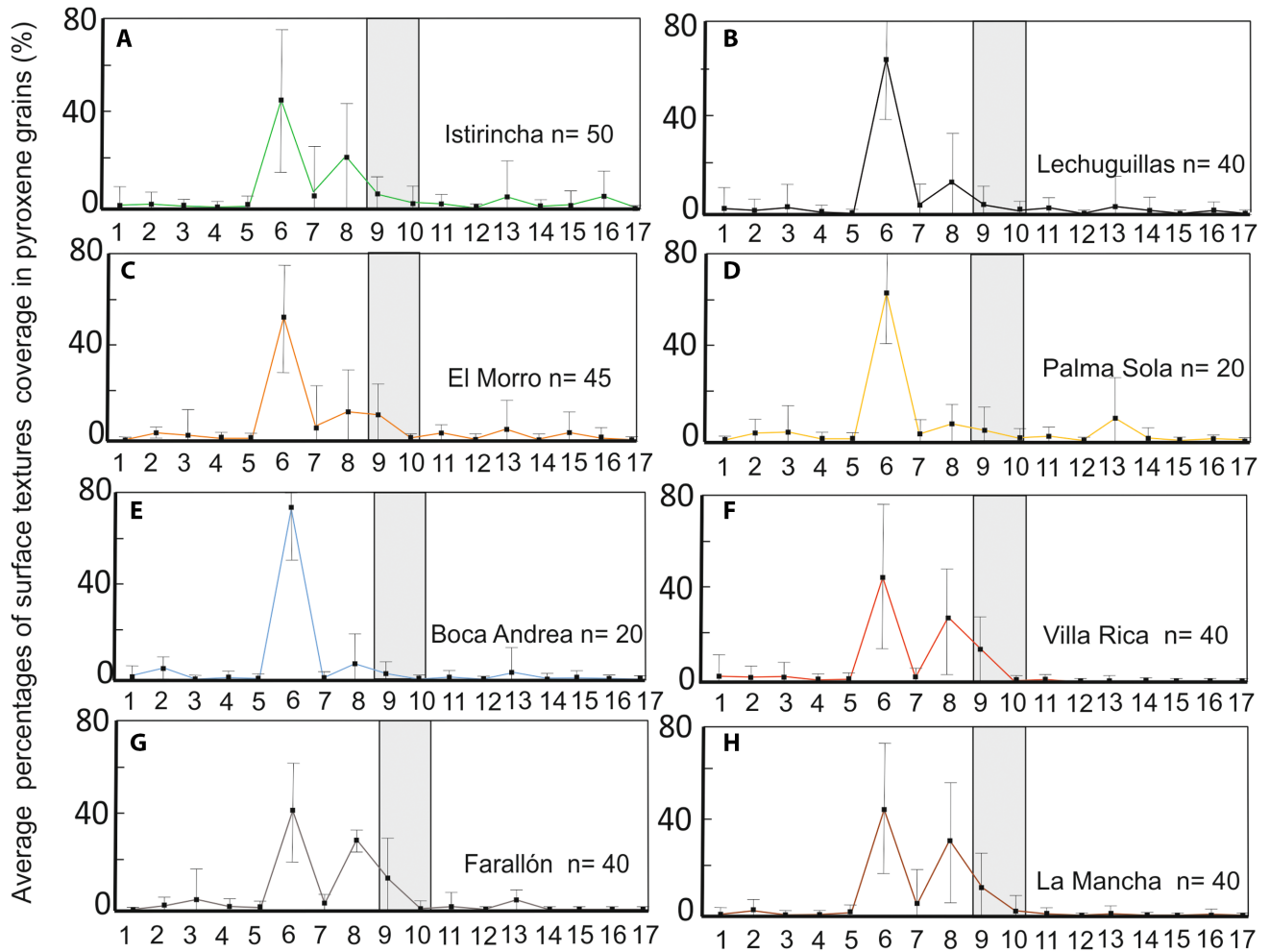
## 5 | DISCUSSION

### 5.1 | Sand petrology

Petrology of the dune sands from the Gulf of Mexico coastal plain is markedly controlled by their closeness

to the Trans Mexican Volcanic Belt and the alluvial deposits in the south-eastern area of the coast. The presence of angular to subrounded monocrystalline quartz largely concentrated in the dune sands suggests that fluvial input, and probably aeolian input, increase quartz with angular and subrounded morphologies, respectively (Mendieta-Lora et al., 2018). However, subrounded quartz commonly occurs in coastal areas like Namibia after fluvial transport (Garzanti et al., 2012). Plagioclase, volcanic fragments with lathwork > micro-lithic > glassy textures and subordinate minerals like ilmenite, andesine, albite, augite and fayalite are derived from intermediate volcanic sources of the Trans Mexican Volcanic Belt (Gómez-Tuena et al., 2007; Mejía-Ledezma et al., 2020; Mendieta-Lora et al., 2018; Negendank et al., 1985). In the study area, plagioclase is commonly embedded within volcanic fragments with lathwork textures but does not occur as single crystals, probably because of the proximity of the source rock. This is similar to volcanic island environments, where plagioclase is more commonly observed in the groundmass of volcanic lithics (Le Pera et al., 2021). The scarcity of olivine grains in the dune sands is probably due to the lack of released monomineralic crystals after rapid fluvial and marine transport. This is suggested by observations from volcanic environments associated with small drainages, where durable retention of olivine occurs in the groundmass of volcanic lithics with glassy textures (Le Pera et al., 2021). This is distinct from the widely held idea that low concentrations of olivine in sands may be a direct consequence of depletion and even elimination of detrital olivine after long subaqueous transport (Garzanti et al., 2015a; Shukri, 1950). Alternatively, the scarcity of olivine grains could be due to their low abundance in the Trans Mexican Volcanic Belt, where differentiated (olivine-poor) igneous rocks are abundant (Gómez-Tuena et al., 2007). Biogenic carbonate grains are deposited as fine-grained fractions during vigorous transport by longshore currents

FIGURE 5 (A through I) Average percentages of surface texture coverage in pyroxene grains versus surface texture classes for each locality; (J) for the whole site. Surface texture classes are 1 = collision point (cp), 2 = remaining particles (abrasion) (rp), 3 = conchoidal (C), 4 = arcuate steps (as), 5 = straight steps (st), 6 = flat cleavage surfaces (fcs), 7 = upturned plates (up), 8 = bulbous edges (be), 9 = elongated depressions (ed), 10 = arcuate/circular/polygonal cracks (acpc), 11 = microbox (mb), 12 = cornflake (ck), 13 = mammillated (mam), 14 = denticulated (den), 15 = imbricated wedge marks (iwm), 16 = lenticular edge pits (lep), 17 = solution pits (sp); n = number of grains.



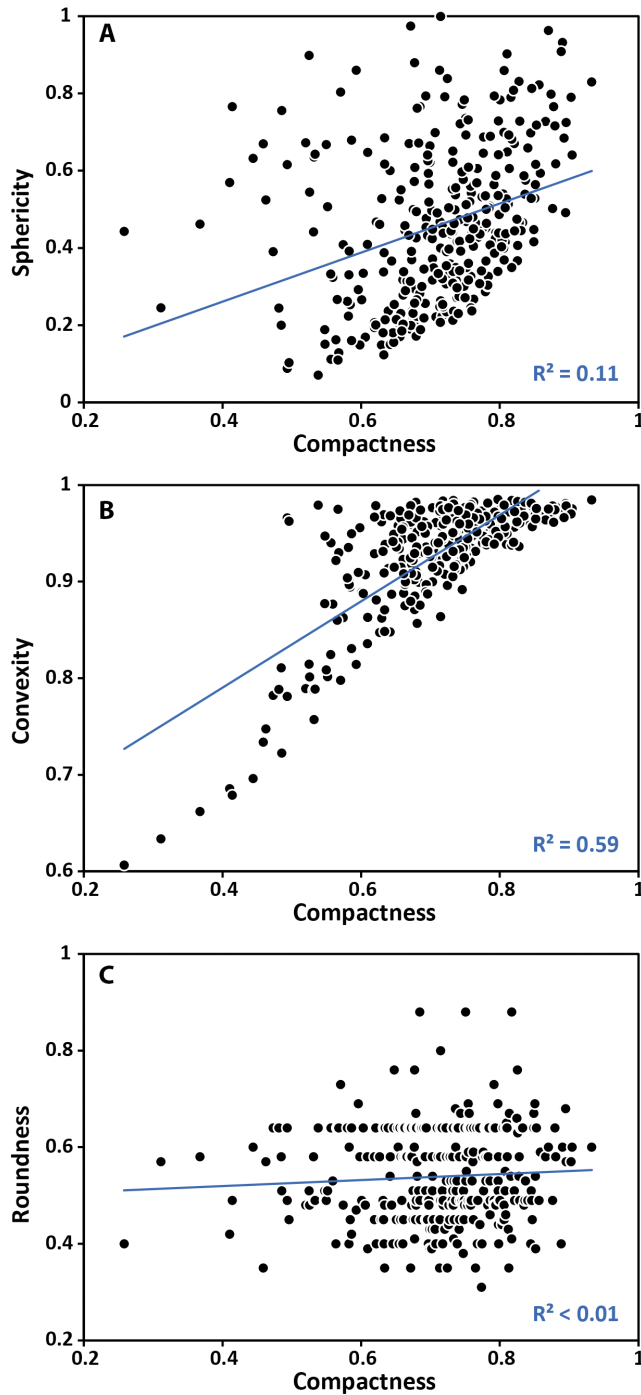


**FIGURE 6** Significant correlations for all sites studied (A) compactness and sphericity, (B) compactness and convexity, and (C) lack of significance between compactness and roundness. Significant correlations  $\rho < 0.05$ .

and winds (Mejía-Ledezma et al., 2020; Mendieta-Lora et al., 2018; Figure 8).

In the Gulf of Mexico coastal sands, the clinopyroxene grains are derived from the sub-alkali to alkali basalts and calcalkaline to tholeiitic basalts originating in the Trans Mexican Volcanic Belt (Ferrari et al., 2005; Gómez-Tuena

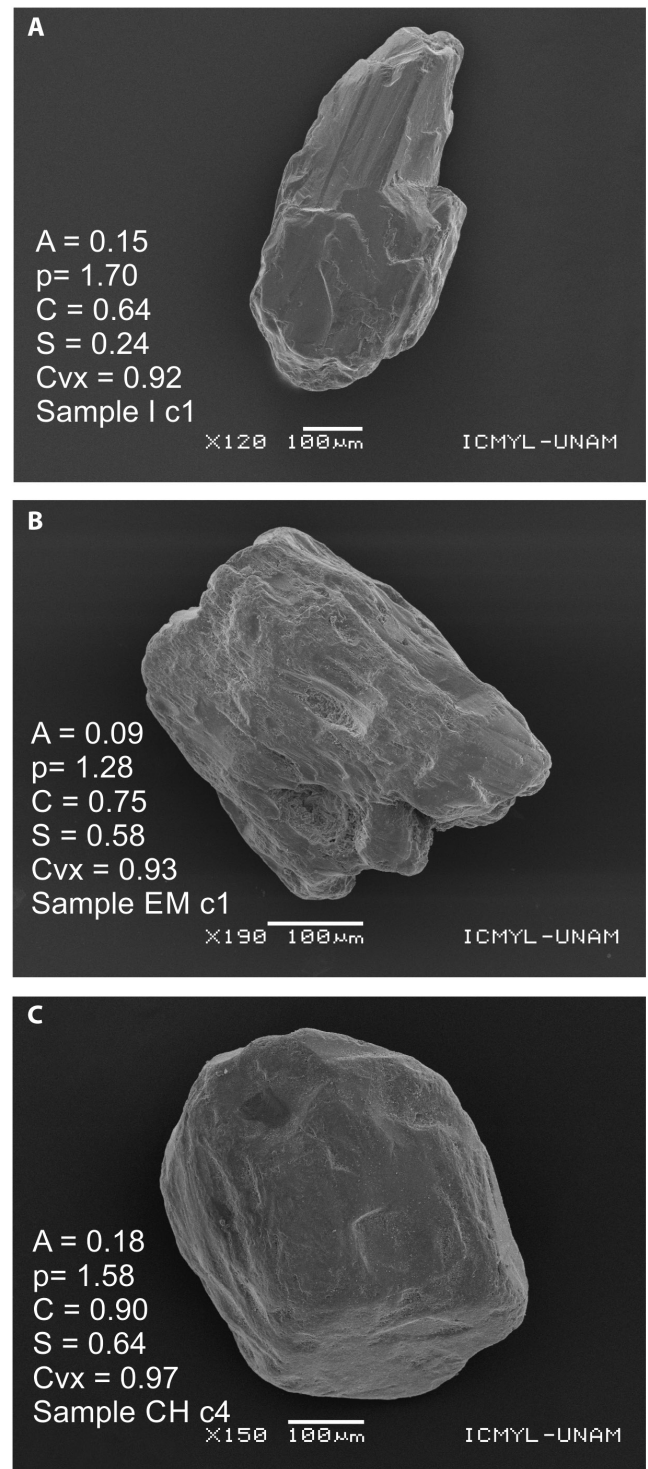


**FIGURE 7** Shape properties in clinopyroxene grains; (A) 'pristine' grain form with a relatively larger area ( $A$ ) and perimeter ( $p$ ) compared to grains B and C. Note the low compactness ( $C$ ) and sphericity ( $S$ ) values in 'elongated' shapes and a constant convexity value ( $Cvx$ ) (Zhao & Wang, 2016). (B) Relative increase in compactness and sphericity values as the grain is less elongated and more compact. (C) Grain with the highest compactness and sphericity values as the grain approaches a semi-developed hexagonal form.

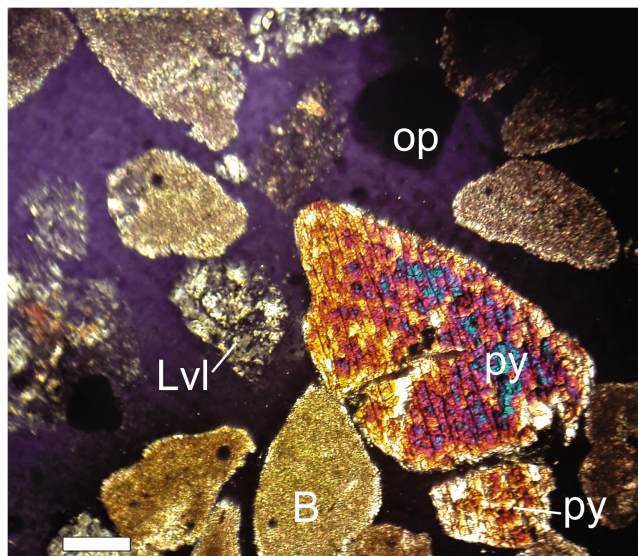


**FIGURE 8** A microphotograph of the whole bulk composition of the dune sands; op= opaques; B= biogenic fractions; py= pyroxenes with angular to subangular outlines; Lvl= volcanic lithics with lathwork texture. Villa Rica site (stoss). Scale bar 500  $\mu\text{m}$ .

et al., 2007; Negendank et al., 1985; Figure 4C,E). The survivability of clinopyroxene in the dune sands is likely a consequence of the proximity of the source rock and rapid fluvial input seaward although detrital pyroxene can sometimes endure after prolonged subaqueous and sub-aerial transport (Garzanti et al., 2012).

## 5.2 | Surface textures on pyroxene grains

### 5.2.1 | Theory

Microtextures on detrital grains can be grouped as mechanical, mechanical/chemical and chemical surface textures. The mechanical surface textures are described as: (i) collision points observed as  $<100\mu\text{m}$  concave/circular holes developed on a cleavage surface probably analogous to elongated depressions but not observed on upturned plates (see Vos et al., 2014); (ii) remaining/granulated particles probably analogous to the abrasion fatigue surface textures formed during vigorous energetic aeolian collisions generating small adhering particles on the surface of the grain (Costa et al., 2013; Mahaney, 2002); (iii) small ( $<50\mu\text{m}$ ), medium ( $<100\mu\text{m}$ ) to large conchoidal ( $>100\mu\text{m}$ ) fractures observed as curved dish-like surface features (Itamiya et al., 2019; Krinsley & Donahue, 1968; Margolis & Krinsley, 1971; Mejía-Ledezma et al., 2020; Moral-Cardona et al., 2005; Vos et al., 2014); (iv) arcuate and (v) straight steps described as curved and linear step-like features present

on conchoidal surfaces and common in coastal dunes and fluvial environments (Itamiya et al., 2019; Mejía-Ledezma et al., 2020; Moral-Cardona et al., 2005; Vos et al., 2014); (vi) flat cleavage surfaces present as breakage patterns (Itamiya et al., 2019; Mejía-Ledezma et al., 2020; Vos et al., 2014); (vii) upturned plates produced as superimposed thin plates (Costa et al., 2013; Itamiya et al., 2019; Krinsley & Cavallero, 1970; Mahaney, 2002; Mejía-Ledezma et al., 2020; Vos et al., 2014); (viii) bulbous edges are observed as well-rounded polished edges (Costa et al., 2013; Krinsley & Doornkamp, 1973; Mahaney, 2002; Mejía-Ledezma et al., 2020; Vos et al., 2014).

The mechanical-chemical surface textures are described as: (ix) elongated depressions present as large dish-shaped concavities (Krinsley et al., 1976; Mahaney, 2002; Mejía-Ledezma et al., 2020; Vos et al., 2014); (x) arcuate/singular/polygonal cracks *ca* 50–100  $\mu\text{m}$  in size and evidence of chemical and mechanical weathering processes (Krinsley & Doornkamp, 1973; Krinsley et al., 1976; Mahaney, 2002; Vos et al., 2014).

The chemical surface textures are described as: (xi) possible microboxwork textures present as boxlike features (Velbel & Barker, 2008); (xii) cornflake particles described as platy-shaped grains (Velbel & Barker, 2008); (xiii) mammillated surface textures were observed as well-developed protuberances exposed on the grain surface of garnets and olivine (Gravenor & Leavitt, 1981; Velbel & Ranck, 2008); (xiv) denticulated surface textures observed as very sharp protuberances (Phillips-Lander et al., 2017; Velbel & Barker, 2008); (xv) imbricated wedge marks produced as the effect of loss of grain surface rather than crystalline overgrowth (Salvino & Velbel, 1989; Velbel et al., 2007); (xvi) lenticular etch pits characterised as a minor concave lens shaped feature  $\leq 20\mu\text{m}$  filled with remaining particles (Velbel & Barker, 2008); and (xvii) solution pits present as small and large holes that vary their size range (*ca* 10 to 100  $\mu\text{m}$ ) (Krinsley & Doornkamp, 1973; Moral-Cardona et al., 2005; Kasper-Zubillaga et al., 2005; Vos et al., 2014; Itamiya et al., 2019; Mejía-Ledezma et al., 2020).

### 5.2.2 | Observation

The visual inspection of clinopyroxene grains provides a catalogue of mechanical mechanical/chemical and chemical surface textures (Figure 9A through O). Hence, mechanical textures develop as collision points (cp) on flat cleavage surfaces (fcs) (Figure 9A,D), remaining/granulated particles (rp) probably associated with abrasion fatigue (Figure 9B), small to large conchoidal fractures (C) (Figure 9C), arcuate (as), straight steps (st) (Figure 9C) and the abundant presence of flat cleavage surfaces

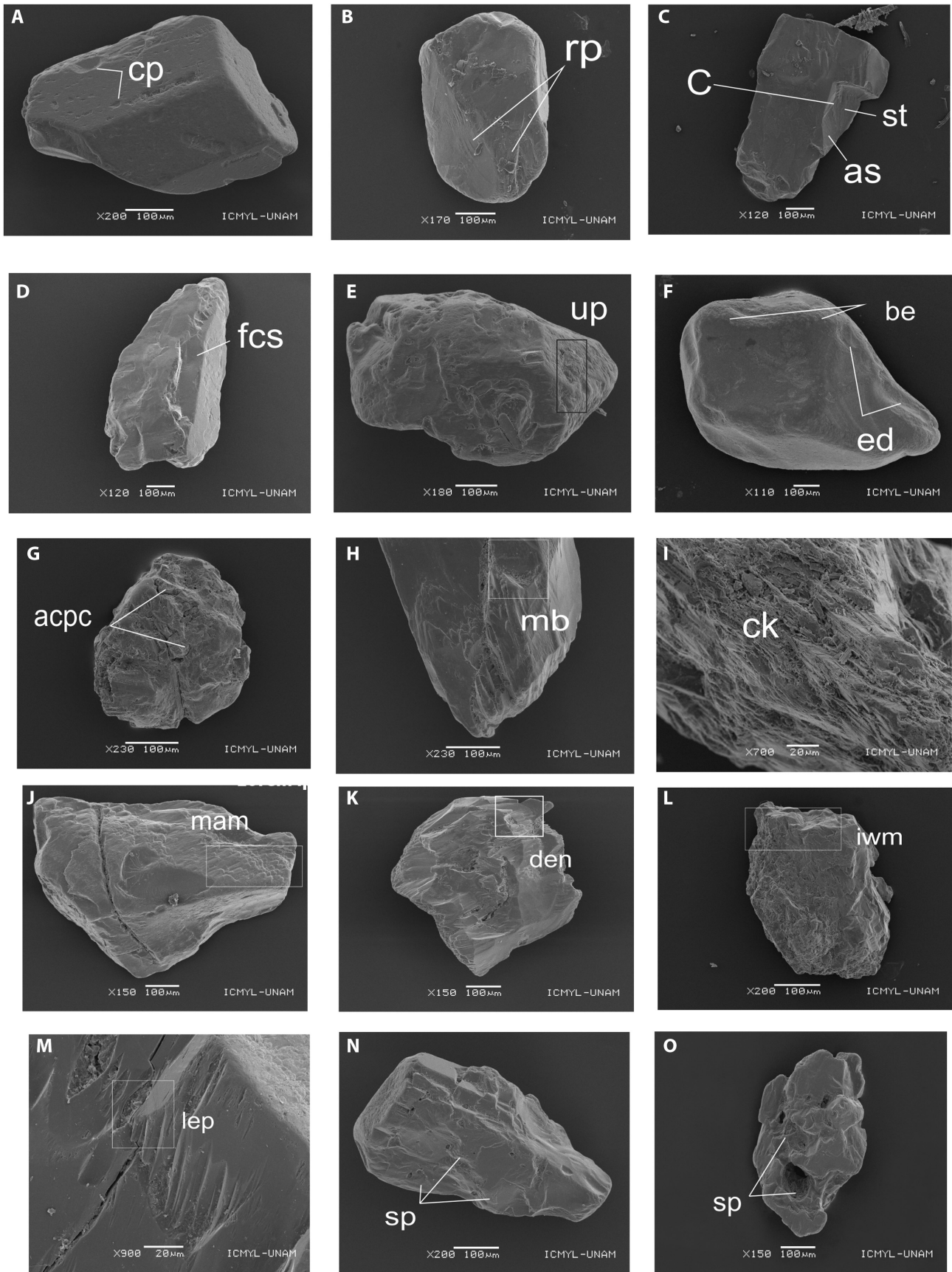


**FIGURE 9** Surface textures catalogued in pyroxene grains: Grain samples are: (A) I-c-2-6, (B) EM-l-2-5, (C) BA-c-6, (D) I-s-1-11, (E) I-c-2-7, (F) CH-s-5-3, (G) PS-s-1-5, (H) I-c-2-5, (I) Le-c-1-2, (J) EM-l-2-3, (K) I-l-1-11, (L) Le-s-1-5, (M) LM-s-3-7, (N) I-s-1-7, (O) PS-c-1-9. Full imagery set available.

(Figure 9D). As observed in quartz and other mineral classes, upturned plates (up) (Figure 9E) and bulbous edges (be) endure on clinopyroxene grains (Figure 9F). Mechanical/chemical surface textures on clinopyroxene grains are dominated by elongated depressions (ed) (Figure 9F) and small arcuate/singular/polygonal cracks (acpc) (Figure 9G). Finally, chemical surface textures are sparse and inherited as microboxwork (mb) (Figure 9H), cornflake particles (ck) (Figure 9I), mammillated (mam) (Figure 9J), denticulated (den) (Figure 9K), imbricated wedge marks (iwm) (Figure 9L), lenticular etch pits (lep) (Figure 9M) and (xvii) solution pits (sp) (Figure 9N,O).

### 5.2.3 | Interpretation

Collision points and remaining particles probably developed following processes similar to those that led to the formation of elongated depressions and abrasion fatigue surface textures observed in quartz (Immonen, 2013; Krinsley & Donahue, 1968; Kuenen, 1960; Vos et al., 2014) and ilmenite (Makvandi et al., 2015; Mejía-Ledezma et al., 2020) from this and other study areas (Costa et al., 2013; Krinsley et al., 1976). Both surface textures are probably produced by high energy collisions during aeolian transport analogous to the abrasion fatigue surface textures resulting from grinding particles (Costa et al., 2013; Mahaney, 2002; Vos et al., 2014).

Larger size conchoidal fractures resulted from a highly active fluvial transport, following a morphological response similar to that commonly observed in other detrital minerals like quartz, ilmenite, garnet and zircon found in modern and ancient sandstones (Kasper-Zubillaga et al., 2005; Madhavaraju et al., 2022; Mejía-Ledezma et al., 2020; Moral-Cardona et al., 2005; Reddad et al., 2016; Varghese et al., 2016). The largest conchoidal fractures were probably generated on large, exposed areas and acquired by the clinopyroxenes during transport and depositional episodes in a similar manner to that observed in coarse-sized quartz grains (Vos et al., 2014). This is because clinopyroxene breaks easily along its flat cleavage surfaces and crystallographic structure. Both physical properties induce the development of large conchoidal fractures during grain-to-grain subaqueous collisions in coarse to medium-fine sands (e.g. poorly sorted sands) (Andò et al., 2012; Folk, 1980; Le Pera & Morrone, 2020; Velbel, 2007; Vos et al., 2014). Arcuate and straight steps commonly reported for quartz, ilmenite, garnet and zircon evolve as features associated with conchoidal fractures (Itamiya et al., 2019; Krinsley & Donahue, 1968; Madhavaraju et al., 2022; Mejía-Ledezma et al., 2020; Moral-Cardona et al., 2005).

Flat cleavage surfaces can form most of the surface texture on detrital clinopyroxene grains due to the high

abundance of weak cleavages in these minerals (Le Pera & Morrone, 2020). As also commonly observed in quartz and ilmenite (Cheng et al., 2017; Itamiya et al., 2019; Mejía-Ledezma et al., 2020; Vos et al., 2014), cleavage surfaces observed in the studied clinopyroxenes indicate they are features produced during high-energy fluvial transport and grain-to-grain collisions in the intertidal zone. However, unlike quartz, flat cleavage surfaces in clinopyroxenes are almost exclusively observed in larger grains (>100 µm).

Upturned plates are surface textures typical of aeolian environments (Costa et al., 2013; Krinsley & Cavallero, 1970; Mahaney, 2002), but they are poorly developed in the studied clinopyroxenes. This suggests that rapid aeolian transport occurs from the beach deposits onto the dunes in the study area, without any time to evolve upturned plates as part of a long-term aeolian process. Alternatively, upturned plates (and other small textures) might have developed on the clinopyroxenes before being removed/obscured during the development of flat cleavage surfaces during aeolian transport. This process could hide some textural features commonly developed during vigorous subaqueous and aeolian multicycles of sand transport. A relatively significant average percentage increase in bulbous edges on the clinopyroxene surfaces at the Chachalacas site is a response to the dominantly aeolian transport with the mineral's physical attributes and larger grain sizes >150 µm (Folk, 1980; Garzanti et al., 2015a; Resentini et al., 2018; Vos et al., 2014). Bulbous edges have also been reported in quartz, ilmenite and zircon from aeolian environments and sandstones (Costa et al., 2013; Mejía-Ledezma et al., 2020; Moral-Cardona et al., 2005).

In summary, surface textures on the studied clinopyroxene grains preserve signals acquired predominantly during subaqueous transport in the fluvial to intertidal beach zone environments, with subsequent minor overprints during subaqueous to aeolian transport to coastal sand dunes. Cleavage breakage is common in larger clinopyroxenes and can obscure the details of these signals.

A mix of physical and chemical processes acting on the grains are represented as elongated depressions derived from the grain-to-grain collisions during sand saltation or creeping (Mahaney, 2002). Commonly, they are preserved together with bulbous edges in grains >150 µm in size.

Arcuate/circular/polygonal cracks result from physical or chemical weathering, including the crystallisation of salts (Krinsley & Doornkamp, 1973; Krinsley et al., 1976; Vos et al., 2014). They can be attributed to minor chemical weathering and/or early diagenesis with a short residence time of the grains under intense chemical weathering conditions. In addition, arcuate/circular/polygonal cracks have not been reported in quartz from coastal sand dunes

(Vos et al., 2014), which may suggest efficient removal of these textures during the breakage and surface abrasion of grains affected by fast-paced multicycle transportation/reworking (Mejía-Ledezma et al., 2020).

There is little evidence of incipient microbox and cornflake textures in the clinopyroxenes (Velbel & Barker, 2008), as chemical weathering is negligible despite their vulnerability to chemical alteration (Buchs et al., 2015; Morton & Hallsworth, 2007). Mammillated surface textures likely reflect subaqueous alteration, where surface material was dissolved to form pinnacle features similar to those observed previously on olivine grains (Grandstaff, 1978; Velbel & Ranck, 2008).

Early stages of weathering are evidenced by the preservation of denticulated surface textures, defined as retreating or remnants of initial void spaces (Velbel & Barker, 2008). In addition, little development of imbricated wedge marks on the surface of the studied clinopyroxene grains suggests that the minerals were affected by the dissolution of their original crystal boundaries rather than grain enlargement produced by crystal overgrowths. Similar observations were previously made for detrital garnet (Salvino & Velbel, 1989; Velbel et al., 2007), suggesting this may be a recurring feature of ferro-magnesian minerals not encountered as commonly in quartz.

Although the abundance of lenticular etch pits increases slightly at the Istrincha sampling site, these textures and solution pits are generally negligible on clinopyroxene grains in the study area. Lenticular etch pits typically result from the formation of pore voids, with the development of vermiform corrosion features within resistant material (Velbel, 2007; Velbel & Barker, 2008). In contrast, solution pits occur during chemical weathering occasionally set on imbricated wedge marks (Velbel et al., 2007).

Overall, limited chemical surface textures on the studied clinopyroxene indicates moderate chemical weathering of grains. Instead, the morphology of retrieved grains was mainly controlled by cleavage breakage and other mechanical features developed during the highly energetic fluvial, marine and aeolian transport of their sedimentary cycle.

### 5.3 | Compactness measurements: Implications of pyroxene breakage

The significant correlation between compactness versus sphericity and convexity values suggests that the shape of the clinopyroxene is controlled by its original form, an irregular polygon, rather than being abraded to adopt a circular form. This is because sphericity accounts for a ratio of the area of the particle related to an enclosed and

inscribed circle and convexity is the ratio of the particle related to the convex hull (polygon). The low average value of sphericity and the high convexity value suggests an irregular shape for the clinopyroxene grains, closer to a polygon rather than a circle (see Zhao & Wang, 2016; Figure 7A–C). Compactness is not correlated to the equivalent diameter or particle size ( $R^2=0.11$ ). Furthermore, since compactness correlation is higher to convexity ( $R^2=0.59$ ) than to sphericity ( $R^2=0.11$ ), it is clear that compactness measurements in the studied pyroxenes are generally determined by the irregular shape of the grain rather than its approximation to a circle. Conversely, compactness is not correlated to roundness. This is due to the fact that compactness is a measure of the global shape of the grain whereas roundness is a mesoscale shape descriptor that only quantifies the sharpness of the grains.

In detail, compactness measurements combine some of the key morphological characteristics associated with the larger-scale shape of the mineral grains. In this study, this is exemplified by changes in the relative control of sphericity and convexity on the compactness values between two groups of localities. At the Boca Andrea, Istrincha and Palma Sola sites, sphericity is poorly correlated to compactness ( $R^2=0.01-0.08$ ), but these two parameters are correlated at the six other studied localities (Figure S1). In contrast, convexity at the Boca Andrea, Istrincha and Palma Sola sites is systematically better correlated to compactness than at other localities ( $R^2=0.70-0.95$  vs  $0.20-0.63$ ) (Figure S2). This supports stronger control of convexity relative to sphericity in the compactness values at Boca Andrea, Istrincha and Palma Sola. Compactness results show that most clinopyroxenes display low compactness (Table 1), suggesting limited abrasion of their edges and possible retention of their original forms despite their susceptibility to abrasion (Folk, 1980; Resentini et al., 2018). However, low compactness values can also be controlled by cleavages in the grains, which can facilitate breakage, rather than significant smooth abrasion, of clinopyroxenes under both subaqueous and subaerial conditions (Folk, 1980; Le Pera & Morrone, 2020). The preservation of surface textures like flat cleavage surfaces is plausible evidence of clinopyroxene breakage. Some grains might have achieved relatively higher compactness (e.g. at sites VR and CH) probably due to long aeolian transport and minor breakage, because clinopyroxene are abraded faster than most other heavy minerals (e.g. amphibole, garnet and zircon; Resentini et al., 2018). Conversely, unlike the results reported here, the behaviour of clinopyroxene along the coastal sands of South-West Africa draws attention since rounded clinopyroxene endures in beach and dune sands even after a long distance of littoral transport and fluvial control of the Orange River

input seaward (Garzanti et al., 2014, figure 2; Garzanti et al., 2018). Alternatively, several studies outline how clinopyroxene endures in different areas with different climates and topographic settings (Garzanti et al., 2021, 2022) with evidence of roundness and preservation of chemical surface textures (Garzanti, et al., 2015a).

However, in this study little evidence of abrasion of clinopyroxene grains remains after high energy subaqueous and subaerial transport. Breakage along clinopyroxene cleavage surfaces is probably the main reason for the low preservation of abraded grains. Nonetheless, these results show that angular to subrounded clinopyroxene grains indicate the dominance of river control over aeolian influence on the grains. Finally, compactness is not correlated to the equivalent diameter or particle size ( $R^2 = 0.11$ ).

## 6 | CONCLUSIONS

Heavy minerals in backshore dunes of the Gulf of Mexico coastal plain are mostly clinopyroxenes (augite and diopside) derived from basalts and andesites of the Trans-Mexican volcanic belt. The cleavage properties of clinopyroxenes determines the low compactness values in clinopyroxene grains with breakage under vigorous subaquatic conditions generating minor abrasion along their edges. Flat cleavage surfaces and bulbous edges represent the dominant average surface coverage percentages of mechanical surface textures on retrieved detrital clinopyroxenes. The former texture suggests highly active fluvial transport and grain-to-grain collisions in the intertidal zone. In contrast, bulbous edges were produced by aeolian transport. In addition, slight preservation of elongated depressions associated with bulbous edges in the clinopyroxenes is produced during high energy aeolian transport. Chemical surface textures are almost non-existent on the studied clinopyroxenes except for rare mammillated surface textures derived from dissolution under subaqueous conditions. The limited preservation of chemical surface textures is probably due to fast and energetic transport during their sedimentary cycle, which led to their morphology being dominated by mechanical processes. Notably, these results clearly show that the cleavage properties of these minerals had a significant control on their shape. In this study, large conchoidal fractures on clinopyroxene  $>100\mu\text{m}$  suggests fluvial transport dominates over intertidal control on the grains. However, cleavage may obscure some surface textures initially developed on the clinopyroxenes as the mineral breaks and its surface remains apparently unaltered. The use of the compactness shape descriptor is an alternative approach

to understanding clinopyroxene behaviour during its source-to-sink history in coastal dune sands since it considers the overall shape of the grain, that is sphericity and convexity, rather than the measurements of the particles based solely on the sphericity or roundness as individual parameters. Compactness measurements of grain particles in the digital domain should be visually inspected referencing a complete catalogue of images to ensure compactness measurements are consistent with the shape of the grain particles leading to a more objective interpretation of the shape of detrital clinopyroxene grains in coastal dune sands.

## ACKNOWLEDGEMENTS

Final draft of the manuscript was completed during a Sabbatical Year at the School of Earth and Environmental Sciences Cardiff University, Wales, United Kingdom. The authors thank PASPA/DGAPA/UNAM for their financial support during the Sabbatical Year's Project 'Preservación del piroxeno en ambientes sedimentarios recientes: Implicaciones geoambientales de su concentración en playas y dunas costeras de México y Nueva Zelandia'. We are truly grateful to Laura Elena Gómez Lizárraga and Carlos Linares López, for Scanning Electron Microscopy and Microprobe Analyses at the Instituto de Ciencias del Mar y Limnología and Laboratorio Universitario de Petrología, Instituto de Geofísica, respectively at the Universidad Nacional Autónoma de México, México. This manuscript has largely benefited from the constructive review by Eduardo Garzanti.

## FUNDING INFORMATION

Universidad Nacional Autónoma de México. Project PASPA/DGAPA/UNAM, México.

## CONFLICT OF INTEREST STATEMENT

The authors declare that they do not have competing financial interest nor conflict of interest.

## DATA AVAILABILITY STATEMENT

Data are available at the following links: <https://hdl.handle.net/20.500.12201/11352>; <https://hdl.handle.net/20.500.12201/11368> (Figure S1); <https://hdl.handle.net/20.500.12201/11369> (Figure S2); <https://hdl.handle.net/20.500.12201/11370> (Figure S3).

## ORCID

Juan J. Kasper-Zubillaga  <https://orcid.org/0000-0002-1169-1359>

## REFERENCES

Alaniz-Alvarez, S., Nieto-Samaniego, A., Morán-Zenteno, D. & Alba-Aldave, L. (2002) Rhyolitic volcanism in extension zone

- associated with strike-slip tectonics in the Taxco region, Southern México. *Journal of Volcanology and Geothermal Research*, 118, 1–14. [https://doi.org/10.1016/S0377-0273\(02\)00247-0](https://doi.org/10.1016/S0377-0273(02)00247-0)
- Andò, S., Garzanti, E., Padoan, M. & Limonta, M. (2012) Corrosion of heavy minerals during weathering and diagenesis: a catalogue for optical analysis. *Sedimentary Geology*, 280, 165–178. <https://doi.org/10.1016/j.sedgeo.2012.03.023>
- Angelidakis, V., Nadimi, S. & Utili, S. (2022) Elongation, flatness and compactness indices to characterise particle form. *Powder Technology*, 396, 689–695. <https://doi.org/10.1016/j.powtec.2021.11.027>
- Armstrong-Altrin, J.S. & Pineda-Olmedo, N. (2014) Microtextures of detrital sand grains from the Tecolutla, Nautla, and Veracruz beaches, western Gulf of Mexico, Mexico: implications for depositional environment and paleoclimate. *Arabian Journal of Geosciences*, 7, 4321–4333. <https://doi.org/10.1007/s12517-013-1088-x>
- Bogaert, J., Rousseau, R., Van Hecke, P. & Impens, I. (2000) Alternative area-perimeter ratios for measurement of 2D shape compactness of habitats. *Applied Mathematics and Computation*, 11, 71–85. [https://doi.org/10.1016/S0096-3003\(99\)00075-2](https://doi.org/10.1016/S0096-3003(99)00075-2)
- Bribiesca, A. (2000) A measure of compactness for 3D shapes. *Computers and Mathematics with Applications*, 40, 1275–1284. [https://doi.org/10.1016/S0898-1221\(00\)00238-8](https://doi.org/10.1016/S0898-1221(00)00238-8)
- Buchs, D.M., Cukur, D., Masago, H. & Garbe-Schönberg, D. (2015) Sediment flow routing during formation of forearc basins: constraints from integrated analysis of detrital pyroxenes and stratigraphy in the Kumano Basin, Japan. *Earth and Planetary Science Letters*, 414, 164–175. <https://doi.org/10.1016/j.epsl.2014.12.046>
- Bufham, B.A. (2000) The size and compactness of particles of arbitrary shape: application to catalyst effectiveness factors. *Chemical Engineering Science*, 55, 5803–5811. [https://doi.org/10.1016/S0009-2509\(00\)00425-5](https://doi.org/10.1016/S0009-2509(00)00425-5)
- Centeno-García, E. (2016) Mesozoic tectono-magmatic evolution of Mexico: an overview. *Ore Geology Reviews*, 1–18, 1035–1052. <https://doi.org/10.1016/j.oregeorev.2016.10.010>
- Chaudhuri, D., Kushwaha, N.K., Sharif, I. & Gohri, V. (2012) Unique measure for geometrical shape object detection-based on area matching. *Defence Science Journal*, 62, 58–66. <https://doi.org/10.14429/dsj.62.942>
- Cheng, Y., Liu, C., Lu, P., Zhang, Y., Nie, Q. & Wen, Y. (2017) Surface textural analysis of quartz grains from modern point bar deposits in lower reaches of the Yellow River. IOP conference series: earth and environmental science <https://doi.org/10.1088/1755-1315/108/3/032023>
- Costa, P.J.M., Andrade, C., Mahaney, W.C., Marques da Silva, F., Freire, P., Freitas, M.C., Janardo, C., Oliviera, M.A., Silva, T. & Lopes, V. (2013) Aeolian microtextures in silica spheres induced in a wind tunnel experiment: comparison with aeolian quartz. *Geomorphology*, 180–181, 120–129. <https://doi.org/10.1016/j.geomorph.2012.09.011>
- Costa, P.J.M., Rasteiro da Silva, D., Figueirinhas, L. & Lario, J. (2019) The importance of coastal geomorphological setting as a controlling factor on microtextural signatures of the 2010 Maule (Chile) tsunami deposit. *Geologica Acta*, 17, 1–10. <https://doi.org/10.1344/GeologicaActa2019.17.4>
- Deer, W.A., Howie, R.A. & Zussman, J. (1992) *An introduction to the rock-forming minerals*. London: The Mineralogical Society, 498 p.
- Delvigne, J. (1990) Hypogene and supergene alterations of orthopyroxene in the Koua Bocca ultramafic intrusion, Ivory Coast. *Chemical Geology*, 84, 49–53. [https://doi.org/10.1016/0009-2541\(90\)90161-Y](https://doi.org/10.1016/0009-2541(90)90161-Y)
- Demant, A. (1979) Vulcanología y petrografía del sector Neovolcánico. *Revista Instituto de Geología*, 7, 39–57.
- Diepenbroek, M., Bartholoma, A. & Ibbeken, H. (1992) How round is round? A new approach to the topic “roundness” by Fourier grain shape analysis. *Sedimentology*, 39, 411–422. <https://doi.org/10.1111/j.1365-3091.1992.tb02125.x>
- Dott, R.H. (2003) The importance of Eolian abrasion in supermature quartz sandstones and the paradox of weathering on vegetation-free landscapes. *The Journal of Geology*, 111, 387–405. <https://doi.org/10.1086/375286>
- Fernández-Eguiarte, A., Gallegos-García, A. & Zavala-Hidalgo, J. (1992) Oceanografía Física (Masas de Agua y Mareas de los Mares Mexicanos) IV.9.1, escala 1: 4000.000, Atlas Nacional de México, Instituto de Geografía, Universidad Nacional Autónoma de México, 1 Chart, Mexico.
- Ferrari, L., Orozco-Esquivel, T., Manea, V. & Manea, M. (2011) The dynamic history of the trans-Mexican volcanic belt and the Mexico subduction zone. *Tectonophysics*, 522–523, 122–149. <https://doi.org/10.1016/j.tecto.2011.09.018>
- Ferrari, L., Tagami, T., Eguchi, M., Orozco-Esquivel, M., Petrone, C., Jacobo-Albarrán, J. & López-Martínez, M. (2005) Geology, geochronology and tectonic setting of late Cenozoic volcanism along the southwestern Gulf of Mexico: the Eastern Alkaline Province revisited. *Journal of Volcanology and Geothermal Research*, 146, 284–306. <https://doi.org/10.1016/j.jvolgeores.2005.02.004>
- Folk, R.L. (1980) *Petrology of sedimentary rocks*. Austin, TX: Hemphill Publishing, p. 182.
- Freeman, H. (1961) On the encoding of arbitrary geometric configurations. *Transactions on Electronic Computers*, 10, 260–268.
- Garzanti, E., Andò, S., Padoan, M., Vezzoli, G. & El Kammar, A. (2015a) The modern Nile sediment system: processes and products. *Quaternary Science Review*, 130, 9–56. <https://doi.org/10.1016/j.quascirev.2015.07.011>
- Garzanti, E., Andò, S., Resentini, A., Vezzoli, G., Lustrino, M., Boni, M. & Vermeesch, P. (2012) Petrology of the Namib Sand Sea: long-distance transport and compositional variability in the wind-displaced Orange Delta. *Earth-Science Reviews*, 112, 173–189. <https://doi.org/10.1016/j.earscirev.2012.02.008>
- Garzanti, E., Capaldi, T., Tripaldi, A., Zarate, M., Limonta, M. & Vezzoli, G. (2022) Andean retroarc-basin dune fields and Pampean Sand Sea (Argentina): provenance and drainage changes driven by tectonics and climate. *Earth Science Reviews*, 231, 104077.
- Garzanti, E., Dinis, P., Vermeesch, P., Andò, S., Hahn, A., Huv, J., Limonta, M., Padoan, P., Resentini, A., Rittner, M. & Vezzoli, G. (2018) Sedimentary processes controlling ultralong cells of littoral transport: placer formation and termination of the Orange sand highway in southern Angola. *Sedimentology*, 65, 431–460. <https://doi.org/10.1111/sed.12387>
- Garzanti, E., Dinis, P., Vezzoli, G. & Borromeo, L. (2021) Sand and mud generation from continental flood basalts in contrasting landscapes and climatic conditions (Paraná – Etendeka conjugate igneous provinces, Uruguay and Namibia). *Sedimentology*, 68, 3447–3475. <https://doi.org/10.1111/sed.12905>
- Garzanti, E., Resentini, A., Andò, S., Vezzoli, G., Preira, A. & Vermeesch, P. (2015b) Physical controls on sand composition and relative durability of detrital minerals during ultra-long distance littoral and aeolian transport (Namibia and southern Angola). *Sedimentology*, 62, 971–996. <https://doi.org/10.1111/sed.12169>

- Garzanti, E., Vermeesch, P., Andò, S., Lustrino, M., Padoan, M. & Vezzoli, G. (2014) Ultra-long distance littoral transport of Orange sand and provenance of the Skeleton Coast Erg (Namibia). *Marine Geology*, 357, 25–36. <https://doi.org/10.1016/j.margeo.2014.07.005>
- Gómez-Tuena, A., Orozco-Esquivel, M.T. & Ferrari, L. (2007) Igneous petrogenesis of the trans-Mexican volcanic belt. In: Alaniz-Álvarez, S.A. & Nieto-Samaniego, Á.F. (Eds.) *Geology of México: celebrating the Centenary of the Geological Society of México*. Geological Society of America Special Paper, Vol. 422. Boulder: The Geological Society of America, pp. 129–181. [https://doi.org/10.1130/2007.2422\(05\)](https://doi.org/10.1130/2007.2422(05))
- Graham, R.L. & Yao, F.F. (1983) Finding the convex hull of a simple polygon. *Journal of Algorithms*, 4, 324–331.
- Grandstaff, D.E. (1978) Changes in surface area and morphology and the mechanism of forsterite dissolution. *Geochimica et Cosmochimica Acta*, 42, 1899–1901. [https://doi.org/10.1016/0016-7037\(78\)90245-4](https://doi.org/10.1016/0016-7037(78)90245-4)
- Gravenor, C.P. & Leavitt, R.K. (1981) Experimental formation and significance of etch patterns on detrital garnets. *Canadian Journal of Earth Sciences*, 18, 765–775. <https://doi.org/10.1139/e81-070>
- Hamill, P.F. & Ballance, P.F. (1985) Heavy mineral rich beach sands of the Waitakere coast, Auckland, New Zealand. *New Zealand Journal of Geology and Geophysics*, 28, 503–511. <https://doi.org/10.1080/00288306.1985.10421203>
- Hyslip, J.P. & Vallejo, L.E. (1997) Fractal analysis of the roughness and size distribution of granular materials. *Engineering Geology*, 48, 231–244. [https://doi.org/10.1016/S0013-7952\(97\)00046-X](https://doi.org/10.1016/S0013-7952(97)00046-X)
- Immonen, N. (2013) Surface microtextures of ice-rafted quartz grains revealing glacial ice in the Cenozoic Arctic. *Palaeogeography, Palaeoclimatology, Palaeoecology*, 374, 293–302. <https://doi.org/10.1016/j.palaeo.2013.02.003>
- Itamiya, H., Sugita, R. & Sugai, T. (2019) Analysis of the surface microtextures and morphologies of beach quartz grains in Japan and implications for provenance research. *Progress in Earth and Planetary Science*, 6, 1–14. <https://doi.org/10.1186/s40645-019-0287-9>
- Johnsson, M.J., Ellen, S.D. & McKittrick, M.A. (1993) Intensity and duration of chemical weathering: an example from soil clays of the southern Koolau Mountains, Oahu, Hawaii. In: Johnsson, M.J. & Basu, A. (Eds.) *Processes controlling the composition of clastic sediments* Geological Society of America, Special Paper, Vol. 284. Boulder: The Geological Society of America, pp. 1–19. <https://doi.org/10.1130/SPE284-p147>
- Kasper-Zubillaga, J.J., Arellano-Torres, E., Álvarez-Sánchez, L.F., Carlos Delgado, L., Martínez-Serrano, R.G. & Baltazar-Jiménez, P.A.E. (2022) Implications of polymodal distributions in the grain size parameters of coastal dune sands (Oaxaca, Mexico). *Sedimentary Geology*, 437, 106189. <https://doi.org/10.1016/j.sedgeo.2022.106189>
- Kasper-Zubillaga, J.J., Carranza Edwards, A. & Rosales-Hoz, L. (1999) Petrography and geochemistry of Holocene sands in the western Gulf of Mexico: implications for provenance and tectonic setting. *Journal of Sedimentary Research*, 69, 1003–1010. <https://doi.org/10.2110/jsr.69.1003>
- Kasper-Zubillaga, J.J., Dickinson, W.W., Carranza Edwards, A. & Hornelas-Orozco, Y. (2005) Petrography of quartz grains in beach and dune sands of Northland, North Island, New Zealand. *New Zealand Journal of Geology and Geophysics*, 48, 649–660. <https://doi.org/10.1080/00288306.2005.9515139>
- Kottek, M., Grieser, J., Beck, C., Rudolf, B. & Rubel, F. (2006). World Map of the Köppen-Geiger climate classification updated 15: 259–263.
- Krinsley, D.H. & Cavallero, L. (1970) Scanning electron microscopic examination of periglacial eolian sands from Long Island, New York. *Journal of Sedimentary Research*, 40, 1345–1350. <https://doi.org/10.1306/74D721A3-2B21-11D7-8648000102C1865D>
- Krinsley, D.H. & Donahue, J. (1968) Environmental interpretation of sand grain surface textures by electron microscopy. *Geological Society of American Bulletin*, 79, 743–748. [https://doi.org/10.1130/0016-7606\(1968\)79\[743:EIOSGS\]2.0.CO;2](https://doi.org/10.1130/0016-7606(1968)79[743:EIOSGS]2.0.CO;2)
- Krinsley, D.H. & Doornkamp, J.C. (1973) *Atlas of quartz sand surface textures*. Cambridge: Cambridge University Press, p. 37.
- Krinsley, D.H., Friend, P.F. & Klimentidis, R. (1976) Eolian transport textures on the surfaces of sand grains of Early Triassic age. *Geological Society of American Bulletin*, 87, 130–132. [https://doi.org/10.1130/0016-7606\(1976\)87<130:ETTOTS>2.0.CO;2](https://doi.org/10.1130/0016-7606(1976)87<130:ETTOTS>2.0.CO;2)
- Krinsley, D.H. & Wellendorf, W. (1980) Wind velocities determined from the surface textures of sand grains. *Nature*, 283, 372–373. <https://doi.org/10.1038/283372a0>
- Kuenen, P.H. (1960) Experimental abrasion: 4. Eolian action. *The Journal of Geology*, 68, 427–449. <https://doi.org/10.1086/626675>
- Le Pera, E. & Morrone, C. (2020) The use of mineral interfaces in sand-sized volcanic rock fragments to infer mechanical durability. *Journal of Palaeogeography*, 9, 21. [doi:10.1186/s42501-020-00068-8](https://doi.org/10.1186/s42501-020-00068-8)
- Le Pera, E., Morrone, C., Arribas, J., Arribas, M.E., Ancochea, E. & Huertas, M.J. (2021) Petrography and provenance of beach sands from volcanic ocean islands: Cabo Verde, Atlantic Ocean. *Journal of Sedimentary Research*, 91, 92–115. <https://doi.org/10.2110/jsr.2020.096>
- Leterrier, J., Maury, R., Thonon, P., Girard, D. & Marchal, M. (1982) Clinopyroxene composition as a method of identification of the magmatic affinities of paleo-volcanic series. *Earth and Planetary Science Letters*, 59, 139–154. [https://doi.org/10.1016/0012-821X\(82\)90122-4](https://doi.org/10.1016/0012-821X(82)90122-4)
- Li, W., Goodchild, M.F. & Churc, C. (2013) An efficient measure of compactness for two-dimensional shapes and its application in regionalization problems. *International Journal of Geographical Information Science*, 27, 1227–1250. <https://doi.org/10.1080/13658816.2012.752093>
- Madhavaraju, J., Armstrong-Altrin, J.S., Selvaraj, K. & James, R.A. (2022) Microtextures on quartz grains from the Gulf of Mexico and the Mexican Pacific coastal sediments: implications for sedimentary processes and depositional environment. *Journal of Palaeogeography*, 11, 256–274. <https://doi.org/10.1016/j.jop.2022.04.001>
- Mahaney, W.C. (2002) *Atlas of sand grain surface textures and applications*. New York: Oxford University Press, p. 237.
- Makvandi, S., Beaudoin, G., McClenaghan, B.M. & Layton-Matthews, D. (2015) The surface texture and morphology of magnetite from the Izok Lake volcanogenic massive sulfide deposit and local glacial sediments, Nunavut, Canada: application to mineral exploration. *Journal of Geochemical Exploration*, 150, 84–103. <https://doi.org/10.1016/j.gexplo.2014.12.013>
- Margolis, S.V. & Krinsley, D.H. (1971) Submicroscopic frosting on eolian and subaqueous quartz sand grains. *Geological Society of*

- American Bulletin*, 82, 3395–3406. [https://doi.org/10.1130/0016-7606\(1971\)82\[3395:SFOEAS\]2.0.CO;2](https://doi.org/10.1130/0016-7606(1971)82[3395:SFOEAS]2.0.CO;2)
- Maria, A. & Carey, S. (2002) Using fractal analysis to quantitatively characterize the shapes of volcanic particles. *Journal of Geophysical Research*, 107, 2283. <https://doi.org/10.1029/2001JB000822>
- Maria, A. & Carey, S. (2007) Quantitative discrimination of magma fragmentation and pyroclastic transport processes using the fractal spectrum technique. *Journal of Volcanology and Geothermal Research*, 161, 234–246. <https://doi.org/10.1016/j.jvolgeores.2006.12.006>
- Marsaglia, K.M. (1993) Basaltic Island sand provenance. In: Johnsson, M.J. & Basu, A. (Eds.) *Processes controlling the composition of clastic sediments Geological Society of America, Special Paper*, Vol. 284. Boulder: The Geological Society of America, pp. 41–65. <https://doi.org/10.1130/SPE284-p41>
- Mejía-Ledezma, R.O., Kasper-Zubillaga, J.J., Álvarez Sánchez, L.F., Mendieta-Lora, M., Arellano-Torres, E., Tetlalmatzi-Marínez, J.L., González-Bermúdez, A., Patiño-Andrade, D. & Armstrong-Altrin, J.S. (2020) Surface textures of quartz and ilmenite grains from dune and beach sands of the Gulf of Mexico coast, Mexico: implications for fluvial, aeolian and marine transport. *Aeolian Research*, 45, 100611. <https://doi.org/10.1016/j.aeolia.2020.100611>
- Mendieta-Lora, M., Mejía-Ledezma, R.O., Kasper-Zubillaga, J.J., Arellano-Torres, E. & Álvarez Sánchez, L.F. (2018) Mineralogical and geochemical implications of weathering rates in coastal dunes and beach sands close to a volcanic rock source in the western Gulf of Mexico, Mexico. *Chemie Der Erde. Geochemistry*, 78, 323–329. <https://doi.org/10.1016/j.chemer.2018.06.004>
- Mo, P.Q. (2020) Internal rolling method for particle shape evaluation and reconstruction. *PLoS One*, 15, e0242162. <https://doi.org/10.1371/journal.pone.0242162>
- Montero, R.S. & Bribiesca, E. (2009) State of the art of compactness and circularity measures. *International Mathematical Forum*, 4, 1305–1335.
- Moral-Cardona, J.P., Gutierrez-Mas, J.M., Sánchez-Bellón, S., Domínguez-Bella, S. & Martínez-López, J. (2005) Surface textures of heavy-mineral grains: a new contribution to provenance studies. *Sedimentary Geology*, 174, 223–235. <https://doi.org/10.1016/j.sedgeo.2004.12.006>
- Morimoto, N., Fabries, J., Ferguson, A.K., Ginzburg, I.V., Ross, M., Seifert, F.A., Zussman, J., Aoki, K. & Gottardi, G. (1988) Nomenclature of pyroxenes. *Mineralogy and Petrology*, 39, 55–76. <https://doi.org/10.1007/BF01226262>
- Morrone, C., Le Pera, E., Marsaglia, K.M. & De Rosa, R. (2020) Compositional and textural study of modern beach sands in the active volcanic area of the Campania region (southern Italy). *Sedimentary Geology*, 396, 105567. <https://doi.org/10.1016/j.sedgeo.2019.105567>
- Morton, A.C. & Hallsworth, C.R. (2007) Stability of detrital heavy minerals during burial diagenesis. In: Mange, M.A. & Wright, D.T. (Eds.) *Heavy minerals in use*. Developments in Sedimentology, Vol. 58. Amsterdam: Elsevier, pp. 215–245. [https://doi.org/10.1016/S0070-4571\(07\)58007-6](https://doi.org/10.1016/S0070-4571(07)58007-6)
- Negendank, J.F.W., Emmermann, R., Krawczyk, R., Mooser, F., Tobschall, H. & Wehrle, D. (1985) Geological and geochemical investigations on the eastern Trans-Mexican Volcanic Belt. *GeofisiInternacional*, 24, 477–575.
- Ortega-Gutiérrez, F., Mitre-Salazar, L.M., Roldán-Quintana, J., Aranda-Gómez, J.J., Morán-Zenteno, D.J., Alaniz-Alvarez, S.A. & Nieto-Samaniego, A.F. (1992) *Carta Geológica de la República Mexicana, Esc. 1:2 000 000, 5a. Edic. y Texto Explicativo*. México DF: Universidad Nacional Autónoma de México. Instituto de Geología y Secretaría de Minas e Industria Paraestatal, Consejo de Recursos Minerales, p. 74.
- Ortiz-Pérez, M.A. & Espinosa, R.L.M. (1991) Clasificación geomorfológica de las costas de México. *Geografía y Desarrollo*, 2, 2–9.
- Osserman, R. (1978) Isoperimetric inequality. *Bulletin of the American Mathematical Society*, 84, 1182–1238.
- Pasquaré, G., Ferrari, L., Garduño, V., Tibali, A. & Vezzoli, L. (1991) Geology of the central sector of the Mexican Volcanic Belt States of Guanajuato and Michoacán. Geological Society of America Maps and Chart Series MCH072, scale 1: 3000 000 1 sheet 22.
- Pereyra Díaz, D., Pérez Sesma, J.A. & Salas Ortega, M.D.R. (2010) Universidad Veracruzana Repositorio Institucional In Gobierno del Estado de Veracruz. *Hidrología Universidad Veracruzana*, 1, 85–122.
- Pérez-Quezadas, J., Cortés-Silva, A., Salas-Ortega, M.R., Araguás-Araguás, L., Pedro Morales-Puente, P. & Carrillo-Chávez, A. (2017) Evidencias hidrogeoquímicas e isotópicas sobre el origen del agua subterránea en la cuenca hidrográfica Río Actopan, Estado de Veracruz. *Revista Mexicana de Ciencias Geológicas*, 3(4), 25–37.
- Pérez-Villegas, G. (1990) *Wind sheet IV.4.2, Vientos dominantes 1:4 000.000*. Mexico: Atlas Nacional de México. Instituto de Geografía, Universidad Nacional Autónoma de México.
- Phillips-Lander, C.M., Legett, C., IV, Elwood Madden, A.S., Megan, E. & Elwood Madden, M.E. (2017) Can we use pyroxene weathering textures to interpret aqueous alteration conditions? Yes and No. *American Mineralogist*, 102, 1915–1921. <https://doi.org/10.2138/am-2017-6155>
- Ramer, U. (1972) An iterative procedure for the polygonal approximation of plane curves. *Computer Graphics and Image Processing*, 1, 244–256. [https://doi.org/10.1016/S0146-664X\(72\)80017-0](https://doi.org/10.1016/S0146-664X(72)80017-0)
- Reddad, H., El Talibi, H., Perri, F., El Moussaoui, S., Zrdeb, M.A., Zaghloul, M.N. & Critelli, S. (2016) Textural and compositional controls on modern fluvial and beach sands of Mediterranean coastal Rif belt (Northern Rif, Morocco). *Italian Journal of Geosciences*, 135, 336–349. <https://doi.org/10.3301/IJG2015.33>
- Resentini, A., Andò, S. & Garzanti, E. (2018) Roundness of detrital minerals by image analysis: sediment transport, shape effects and provenance implications. *Journal of Sedimentary Research*, 88, 276–289. <https://doi.org/10.2110/jsr.2018.12>
- Roduit, N. (2007). JMicroVision: un logiciel d'analyse d'images pétrographiques polyvalent. Unpublished PhD Thesis, Université de Genève, Switzerland. 116.
- Roduit, N. (2019) JMicroVision: image analysis toolbox for measuring and quantifying components of high-definition images. Version 1.3.1. <https://jmicrovision.github.io>
- Rosenfeld, A. (1974) Compact figures in digital pictures. *IEEE Trans Systems, Man and Cybernetics*, 4, 221–223.
- Salvino, J.F. & Velbel, M.A. (1989) Faceted garnets from sandstones of the Munising Formation (Cambrian), northern Michigan: petrographic evidence for their origin by intrastratal dissolution. *Sedimentology*, 36, 371–379. <https://doi.org/10.1111/j.1365-3091.1989.tb00613.x>

- Schott, J., Berner, R.A. & Sjöberg, E.L. (1981) Mechanism of pyroxene and amphibole weathering-I. Experimental studies of iron-free minerals. *Geochimica et Cosmochimica Acta*, 45, 2123–2135. [https://doi.org/10.1016/0016-7037\(81\)90065-X](https://doi.org/10.1016/0016-7037(81)90065-X)
- Servicio Geológico Mexicano. (2017) Cartografía Geológica De La República Mexicana. Geological Chart. Formato SHP Escala 1:250,000.
- Shukri, N.M. (1950) The mineralogy of some Nile sediments. *Quarterly Journal of the Geological Society of London*, 105, 511–534.
- Tamayo, J.L. (2013) *Geografía Moderna de México*. México: Trillas, p. 390.
- Tejeda Martínez, A., Acevedo, F. & Jáuregui, E. (1988) *Atlas Climático del Estado de Veracruz*. Mexico: Universidad Veracruzana, p. 150.
- Thomas, M.C., Wiltshire, A.T. & Williams, A.T. (1995) The use of Fourier descriptors in the classification of particle shape. *Sedimentology*, 42, 635–645. <https://doi.org/10.1111/j.1365-3091.1995.tb00397.x>
- Varghese, T.I., Prakash, T.N. & Nagendra, R. (2016) Depositional history of coastal plain sediments, Southern Kerala, South West India. *Journal of Earth Science & Climatic Change*, 7, 6. <https://doi.org/10.4172/2157-7617.1000355>
- Velbel, M.A. (2007) Surface textures and dissolution processes of heavy minerals in the sedimentary cycle: examples from pyroxenes and amphiboles. In: Mange, M.A. & Wright, D.T. (Eds.) *Developments in Sedimentology*, Vol. 58. Amsterdam, pp. 113–150.
- Velbel, M.A. & Barker, W.W. (2008) Pyroxene weathering to smectite: conventional and cryo-field emission scanning electron microscopy, Koua Bocca ultramafic complex, Ivory Coast. *Clays and Clay Minerals*, 56, 112–127. <https://doi.org/10.1346/CCMN.2008.0560110>
- Velbel, M.A., McGuire, J.T. & Madden, A.S. (2007) Scanning electron microscopy of garnet from southern Michigan soils: etching rates and inheritance of preglacial and pre-pedogenic grain-surface textures. *Developments in Sedimentology*, 58, 413–432.
- Velbel, M.A. & Ranck, J.M. (2008) Etch pits on naturally altered olivine from dunites of the Appalachian Blue Ridge Mountains, North Carolina, USA. *Mineralogical Magazine*, 72, 145–148. <https://doi.org/10.1180/minmag.2008.072.1.145>
- Vos, K., Vandenberghe, N. & Elsen, J. (2014) Surface textural analysis of quartz grains by scanning electron microscopy (SEM): from sample preparation to environmental interpretation. *Earth-Science Reviews*, 128, 93–104. <https://doi.org/10.1016/j.earscirev.2013.10.013>
- Vossepoel, A.M. & Smeulders, A.W.M. (1982) Vector code probability and metrication error in the representation of straight lines of finite length. *Computer Graphics Image Processing*, 20, 347–368.
- Wadell, H. (1932) Volume, shape and roundness of rock particles. *Journal of Geology*, 40, 443–451.
- Zhao, B. & Wang, J. (2016) 3D quantitative shape analysis on form, roundness, and compactness with  $\mu$ CT. *Powder Technology*, 291, 262–275. <https://doi.org/10.1016/j.powtec.2015.12.029>
- Zhou, B., Wang, J. & Wang, H. (2018) Three-dimensional sphericity, roundness and fractal dimension of sand particles. *Geotechnique*, 68, 18–30. <https://doi.org/10.1680/jgeot.16.P.20>

## SUPPORTING INFORMATION

Additional supporting information can be found online in the Supporting Information section at the end of this article.

**How to cite this article:** Kasper-Zubillaga, J.J., Martínez-Serrano, R.G., Buchs, D.M., Mendieta-Lora, M., Arellano-Torres, E. & Álvarez-Sánchez, L.F. (2023) Surface textures of detrital pyroxenes in coastal dune sands (western Gulf of Mexico, Mexico): Implications for their preservation and geoenvironmental processes. *The Depositional Record*, 00, 1–21. <https://doi.org/10.1002/dep2.228>